

Study of Anatase Nanofluid Droplet Impingement on Superhydrophobic Surface

Thesis submitted towards partial fulfilment of the requirements for the award of
the Degree of Master of Technology in Nano Science and Technology

By

SURJAYAN BISWAS

Registration number: 160447 of 2021-22

Class Roll No: 002130701026

Examination Roll No: M4NST23005

Under the guidance of **Prof. Swarnendu Sen, Prof. Ranjan Ganguly
& Prof. Apurba Kumar Santra**

School of Materials Science and Nanotechnology

Jadavpur University

Kolkata-700032

INDIA.

June 2023

**School of Materials Science and Nanotechnology
Jadavpur University
Kolkata- 700032
INDIA.**

CERTIFICATE OF RECOMMENDATION

We hereby recommend that the thesis entitled as "Study of Anatase Nanofluid Droplet Impingement on Superhydrophobic Surface", prepared by **Mr. Surjayan Biswas** (Class Roll No:002130701026, Registration No. 160447 of 2021-22, Examination Roll No. M4NST23005) under our guidance, be accepted in partial fulfilment of the requirement for the award of the Degree of Master of Technology in Nano Science and Technology from the School of Materials Science and Nano Technology of Jadavpur University.

HOD / Director
Dr. Sourav Sarkar
Director,
School of Materials Science and Nano
Technology,
Jadavpur University

Thesis Advisor
Dr. Swarnendu Sen
Professor,
Department of Mechanical Engineering,
Jadavpur University

Thesis Advisor
Dr. Ranjan Ganguly
Professor,
Department of Power Engineering,
Jadavpur University

Thesis Advisor
Dr. Apurba Kumar Santra
Professor,
Department of Power Engineering,
Jadavpur University

Dean-FISLM,
Jadavpur University,
Kolkata – 700 032

School of Materials Science and Nano Technology
Jadavpur University
Kolkata-700032
INDIA.

CERTIFICATE OF APPROVAL

The foregoing thesis titled “**Study of Anatase Nanofluid Droplet Impingement on Superhydrophobic Surface**” was hereby approved by the committee of the final examination for evaluation of the thesis as a credited study of an engineering subject carried out and presented by **Mr. Surjayan Biswas** (Class Roll No: 002130701026, Registration No. 160447 of 2021-22, Examination Roll No. M4NST23005) in a manner satisfactory to warrant its acceptance as a prerequisite to the degree of Master of Technology in Nano Science and Technology. It was understood by this approval, the undersigned do not necessarily endorse or approve any statement made, opinion expressed or conclusion drawn therein but approve the thesis only for the purpose for which it was submitted. Committee of final examination for evaluation of thesis.

Signature

Date

**School of Materials Science and Nano Technology
Jadavpur University
Kolkata- 700032
INDIA.**

Declaration of Originality and Compliance of Academic Ethics

I hereby declare that this thesis titled "**Study of Anatase Nanofluid Droplet Impingement on Superhydrophobic Surface**" contains literature survey and original research work by the undersigned candidate, as part of my Degree of Master of Technology in Nano Science and Technology.

All Information in this document has been obtained and presented in accordance with academic rules and ethical conduct.

I also declare that, as required by these rules and conduct, I have fully cited and referenced all material results that were not original to this work.

.

Name (Block Letters): SURJAYAN BISWAS
Class Roll No: 002130701026
Registration No: 160447 of 2021-22
Examination Roll No: M4NST23005

Signature with date

Acknowledgement

I am overwhelmed in all humbleness and gratefulness to acknowledge my depth to all those who have helped me to put these ideas, well above the level of simplicity and into something concrete.

I would like to express my gratitude to my guide, Professor **Swarnendu Sen** for his strong support, patience and constant availability for technical discussions. I would like to express my particular gratitude to another guide, Professor **Ranjan Ganguly** for being my well-wisher and rendering continuous support, guidance and ideas during my thesis work. I would like to express my sincere gratitude to another guide, Professor **Apurba Kumar Santra**, for his constant patience, guidance and ideas without which completion of this thesis would have been impossible. I am grateful to all Ph.D. Scholars (AMRA Lab) and my fellow M.Tech. Researchers and Juniors I worked with for guiding me during the entire course of research work with their valuable suggestions, support and knowledge.

I would like to thank all the faculty members of **School of Materials Science & Nanotechnology, Jadavpur University, Kolkata**, for giving me the opportunity to carry out my M.Tech thesis work.

I render my heartiest thanks to the faculty members of **Department of Power Engineering, Faculty of Engineering and Technology, Jadavpur University, Kolkata** for giving me opportunity working in **Advance Materials & Research Application Lab** where I got resourceful guidance and proper research environment which has helped me to complete the thesis work more effectively and efficiently.

I would like to thank my **Seniors, Juniors** as well as my **Batchmates** from **School of Materials Science & Nanotechnology** and **Department of Power Engineering, Faculty of Engineering and Technology, Jadavpur University, Kolkata** for their moral supports throughout the duration of the thesis work.

Most of all, my deepest appreciation goes to **My Parents** for their faith, unyielding unconditional love, support, encouragement and quiet patience.

- Surjayan Biswas

Table of Contents

1. Introduction.....	1
1.1 Motivation	1
1.2 Nanofluids	2
1.2.1 Surface Tension of Nanofluids	3
1.3 Literature review	10
1.3.1 Effect of Hydrophilic Nanoparticles on Droplet impingement	12
1.3.2 Effect of Hydrophobic Nanoparticles on Droplet impingement	16
1.3.3 Energy dissipation due to Particle rebound	20
1.3.4 Effect on Weber Number	21
1.3.5 Pinning effect due to Nanoparticles	23
1.4 Gap Area.....	26
1.5 Objectives.....	27
2. Materials and Methods.....	27
2.1 List of Equipment and Materials Used	27
2.1.1 Equipment Used.....	27
2.1.2 Materials Used	28
2.2 Forming of Superhydrophobic plate	28
2.3 Synthesis of Nanofluid.....	30
2.3.1 Two Step Method	30
2.3.2 Measurement of Nanoparticle.....	31
2.3.3 Mixing and Sonication for preparation	32
2.3.4 Surfactant	32

2.4 Surface Tension of Nanofluids	35
2.5 Experimental setup and procedure	37
Table 2.5 Dispensed volume of droplets for different fluids	40
Table 2.5a For Base fluid.....	40
Table 2.5b For 0.01vol% TiO ₂ -CTAB Nanofluid	41
Table 2.5c For 0.1vol% TiO ₂ -CTAB Nanofluid.....	41
Table 2.5d For 0.5vol% TiO ₂ -CTAB Nanofluid	41
3. Results and discussions	42
3.1 Surface Tension of Nanofluids	42
3.1.1 Surface Tension variation with concentration of Nanofluids	42
Table 3.1 Surface Tension variation with concentration of Nanofluids	42
3.2 Impingement dynamics of Nanofluid droplets over Superhydrophobic surface 43	
3.2.1 Effect of droplet diameter, impact Weber number and Parametric variation .	46
Table3.3a: Droplet impinging data for the base fluid.....	46
Table 3.3b: Droplet impinging data due to 0.01vol% Nanofluid	47
Table 3.3c: Droplet impinging data due to 0.1vol% Nanofluid.....	49
Table 3.3d: Droplet impinging data due to 0.5vol% Nanofluid	50
Table 3.3e: Crowning and splashing events for different concentration of fluids	52
3.2.2 Impingement characteristics	51
3.2.2a Impingement characteristics for base fluid	51
3.2.2b Impingement characteristics for 0.01vol % Nanofluid.....	54
3.2.2c Impingement characteristics for 0.1vol % Nanofluid	55
3.2.2d Impingement characteristics for 0.5vol % Nanofluid	55

3.2.3 Spread factor vs Weber number characteristic curves	56
3.2.3a Spread factor vs Weber number characteristic curve for base fluid	56
3.2.3b Spread factor vs Weber number characteristic curve for 0.01 vol% nanofluid	57
3.2.3c Spread factor vs Weber number characteristic curve for 0.1vol% nanofluid	58
3.2.3d Spread factor vs Weber number characteristic curve for 0.5vol% nanofluid	60
4. Conclusions and future directions.....	61
4.1 Conclusions	61
4.2 Scope of future directions	62
5. References.....	63

List of figures

Fig. 1.2.1i Surface tension σ vs concentration C at 23 °C	4
Fig. 1.2.1ii Surface tension of 1 mmol/L CTAB and 2.8 mmol/L LHS solutions vs temperature.....	4
Fig. 1.2.1iii Monolayer partitioning of microscopic droplets	5
Fig. 1.2.1iv Variation of surface tension of surfactant-polymer solutions with the increase in surfactant concentration, at a fixed polymer concentration	6
Fig. 1.2.1v Variation of surface tension of surfactant-polymer solutions with the increase in surfactant (Alfonic 1412-3 Ethoxylate) concentration, at a fixed polymer (CMC) concentration of 500 ppm	7
Fig. 1.2.1vi Surface tension of nanofluids as a function of volume concentration at 25°C	8
Fig. 1.2.1vii Surface tension of DI water+NaBDSwater+NaBDS and surface tension of p-SWNTs nanofluid with NaBDS.....	8
Fig. 1.2.1viii Surface tension variation with nanoparticle concentration for n-decane based nanofluids	9
Fig. 1.3i Droplet dynamics illustration	11
Fig. 1.3ii Normalised droplet diameter over time for water and 0.5% w/w concentration nanofluid droplets impinging onto an uncoated surface	13
Fig. 1.3iii Evolution of droplets containing hydrophilic SiO ₂ particles after impacting on a solid surface (a) Evolution images of droplets (b) Dimensionless height of spreading drops, H/D_0 (c) Dimensionless radius of spreading drops, D/D_0	14
Fig. 1.3iv a) Liquid droplet of lateral radius r and contact angle θ at a substrate – vapor surface (b) In the immediate vicinity of the three-phase SLV contact line, the liquid thickness $l(x)$ varies with distance x along the substrate	15
Fig. 1.3v Evolution of droplets containing hydrophobic SiO ₂ particles after impacting on a solid surface (a) Evolution images of drops (b) Dimensionless height of spreading drops, H/D_0 (c) Dimensionless radius of spreading drops, D/D_0	16

Fig. 1.3vi Measured shear viscosity with respect to shear rate	18
Fig. 1.3vii (a) Variation in viscosity with shear rate of SiO ₂ suspensions (b) Variation in viscosity with particle concentration in shear steady state	18
Fig. 1.3viii The evolution of droplets containing hydrophobic SiO ₂ particles at a concentration of 0.3 wt% post-impact on a solid surface under different Weber number	21
Fig. 1.3ix (a) Dimensionless maximum recoiling height (H_{max}/D_0) (b) Dimensionless maximum spreading radius (D_{max}/D_0) for droplets with hydrophobic particles at a concentration of 0.3 wt%	22
Fig. 1.3x Regime map for contact line pinning as a function of the Weber number and hydrophobic particle concentration.....	23
Fig. 1.3xi Regime map for whole contact line pinning as a function of the Weber number. The normal situation means the contact line retracts immediately	23
Fig. 1.3xii Schematic illustration of the effect of hydrophobic nanoparticles on the dynamics of droplet impacts. F_k is the retracting inertia force, $F_{viscous}$ is the viscous resistance and F_f is the contact line friction force	24
Fig. 2.2i Superhydrophobic surface	29
Fig. 2.3.2i Electronic Balance	31
Fig. 2.3.3 (i) Magnetic stirrer (ii) Magnetic stirring rods	32
Fig. 2.3.4(i) TiO ₂ Nanoparticles (ii) CTAB	34
Fig. 2.3.4 TiO ₂ -CTAB Nanofluids (iii) $\phi=0.01$ (iv) $\phi=0.1$ (v) $\phi=0.5$	34
Fig. 2.3.4 CTAB-water solution (vi) 0.12548 mmol/L (vii) 1.14153 mmol/L (viii) 6.19983 mmol/L	36
Fig. 2.4(i) Surface Tensiometer (ii) Du-Noüy phenomena.....	36
Fig. 2.5i Experimental setup	37
Fig. 2.5ii Bath sonication	38

Fig. 2.5iii (a) Blue needle (Diameter: 0.714mm) (b) Yellow needle (Diameter: 0.231mm) (c) Purple needle (Diameter: 0.540mm)	39
2.5iv (a) Vision research AMTEK Phantom high speed camera (b) Nikon AF NIKKOR 50mm 1:14D camera lens (c) XIT Extension tube.....	40
Fig. 3.2i Impact dynamics of a 0.24cm diameter nanofluid droplet (0.5 vol%, Weber Number 131.62) (a)-(f) shows different stages of dynamics over superhydrophobic surface	43
Fig. 3.2ii Impact dynamics of a 0.24mm diameter nanofluid droplet (0.5 vol%, Weber Number 427.75) (a)-(f) shows different stages of dynamics over superhydrophobic surface	44
Fig. 3.2iii Impact dynamics of a 0.24mm diameter nanofluid droplet (0.5 vol%, Weber Number 493.56) (a)-(f) shows different stages of dynamics over superhydrophobic surface	45
Fig. 3.2.3i (a) Spread factor vs Weber number for all kinds of needles used for base fluid (b) Spread factor vs Weber number for all needles combined used for base fluid	57
Fig. 3.2.3ii (a) Spread factor vs Weber number for all kinds of needles used for 0.01vol% nanofluid (b) Spread factor vs Weber number for all needles combined used for 0.01vol% nanofluid	58
Fig. 3.2.3iii (a) Spread factor vs Weber number for all kinds of needles used for 0.1vol% nanofluid (b) Spread factor vs Weber number for all needles combined used for 0.1vol% nanofluid	59
Fig. 3.2.3iv (a) Spread factor vs Weber number for all kinds of needles used for 0.5vol% nanofluid (b) Spread factor vs Weber number for all needles combined used for 0.5vol% nanofluid	60

Abstract

The prospect of Nano Science and Nanotechnology in various emerging fields has led to the design, synthesis, manipulation and optimization of nanoparticles (1nm-100nm) in order to create new opportunities for the utilization of smaller and more regular structures for various applications. Nanofluids are the new class of fluid made by homogeneously suspending nanometre sized particles in the base liquids like water, ethylene glycol, etc. Nanofluid droplet impacting on a solid surface is a common phenomenon in our everyday life which shows prospects in various applications ranging from assessing the efficacy of a pesticide spray to the clarity of inkjet printing. Different parameters like surface wettability and roughness, surface tension, viscosity and nanoparticle concentration of the liquid, impinging velocity and impacting diameter of the droplet play their respective roles in dictating the outcome of droplet impact on surfaces. It is well-reported in literature that inertia, capillary and viscous forces comes into play as a liquid droplet impacts a solid surface. Akin to the impact of a regular fluid droplet on a flat superhydrophobic surface, a nanofluid droplet would also spread – taking a pancake shape – to a maximum diameter, and then would recede, splash or fragment. Depending upon the impacting droplet momentum, the droplet after impact may again bounce-off. However, several features of nanofluid droplet impact have remained unanswered. For example, the influence of nanofluid particle concentration on the salient impacting behaviors, e.g., maximum droplet spreading diameter, extent of peripheral ring formation, splashing and rebounds of impacted droplets have not been well-investigated. Types of pancake formed after spreading, and its size (diameter) depend on many variables like type and size of nanoparticles, the host fluids, particles volume fraction, nature of surfactant, stabilizing time, impinge velocity, height of impingement, surface wettability, impact of surface roughness, which needs careful study.

In this pursuit, the present work focuses on Anatase (Titanium (IV) oxide nanoparticles of <25nm size, dispersed in deionized water) nanofluid droplet impact behavior on superhydrophobic substrates. Upon impact, pancake-shaped spreading of the nanofluid droplet were observed, with the spreading diameter varying with the droplet dispensing needle diameter and the drop impact velocity (the drop release height). Nanoparticle volume fraction $\phi=0.01\%$, 0.1% and 0.5% were considered in this experiment. The surfactant used here was Cetyl Trimethyl Ammonium Bromide (CTAB). Results of nanofluid droplet impingement are

compared with the impact characteristics of a deionized water droplet. Three needles of internal diameter of 0.714 mm , 0.560 mm and 0.231 mm were used for dispensing the droplets from different heights. It was observed that small droplets (dispensed from small size needle) show fully splashing behaviour at lower Weber number. Droplets dispensed from intermediate size nozzle show splashing at higher Weber number, while splashing occurs at intermediate Weber numbers for the large droplets. Similar experiments were performed by varying the nanoparticle loading. It was observed that with increase in particle loading, the smallest-diameter droplets showed the least Weber number for which the nanodroplet splashes, while the droplet with the highest diameter shows the highest Weber number.

Chapter 1

1. Introduction

1.1 Motivation:

Droplet splashing is an everyday phenomenon in our daily lives. But we don't realise how much it impacts the Engineering applications around us. Though lots of research has been done over years, a lot of challenges and gaps still exist in this field. Droplet splashing refers to a phenomenon where the droplet when released from certain height splashes and satellite droplets are formed. Below that height, the droplet does not splash. However, when height is increased, an impinging effect is noticed as if the surface pushes the droplet and frequency of lamella increases and at a certain height it seems the inertial force by the surface suppresses the potential energy of the droplet. This phenomenon is of immense importance in terms of Engineering applications. We can use water as base fluid without any kind of particle loading. The application includes self-cleaning applications for dust removal or spray cooling for high power systems like advanced lasers or turbines in power plants. There are plenty of other applications where we can implement these phenomena like electronic cooling, fire extinguishing, ink jet printing or direct fuel injection. However, this study will only focus on droplet dynamics, splashing. An effective way of spray cooling can be introduced by using advanced materials like nanoparticles which is capable of heat removal in a more efficient way. It is because the performance of heat transfer using conventional fluids has been in use for long. Reduction in size continuously and demand for high-end performance of electronic devices cause an uptrend in heat flux generation. Consequently, conventional cooling methods using conventional fluids are becoming insufficient in satisfying these cooling need particularly for smaller and higher capacity electronics which requires more effective cooling, creating an opportunity for further progress in the microelectronics industry. So here is where application of Nanofluids come into play. Nanofluids were new class of fluid and it was prepared by mixing nanometer size particles to the base fluid and. The stability of Nanofluid however depends on the type of surfactant used and the volume fraction of Nanoparticle and also the compound otherwise settling of particles pose a severe maintenance problem. Recent studies have shown that change of heat transfer characteristics may be attributed to the deposition of nanoparticles on the heated

surface during nucleation followed by boiling, enhancing the surface properties including the wettability and the capillarity. The increase in nanoparticle volume fraction causes surface tension drop and enlargement of the initial perimeter, reducing the initial equilibrium contact angle. Higher concentration of nanoparticles in fluid results in larger droplet contact areas, thus enhancing heat transfer. Nowadays, Nanofluids are being preferred over traditional heat transfer fluid, which shows higher thermal conductivities. [1] Nanofluids are elemental in the application of combining inkjet printing with nanofluids. It is used to print metallic inks on soft substrates or other special materials for the photovoltaic film, flexible electronics. Nanofluids possesses immense potential. It is a solve for conventional fluids which cannot help a lot with technological advancements. The wetting behaviours can fabricate functional surfaces with coatings through ink-printing for enhancing heat transfer or reducing the drag in micro/bio fluid systems, or enhancing boiling or condensation phase changes. Nanofluids are providing customizable materials by changing nanoparticles or base fluid and it can be expected that the combination of ink-printing and nanofluids welcomes a breakthrough for high precision manufacturing. [2] This particular work emphasizes the bouncing, splashing, receding of Nanofluidic droplet on Super-hydrophobic surfaces and its variation with needle size and particle loading.

1.2Nanofluids:

When nanometre sized particles (1-100nm) are engineered within a base fluid then Nanofluids are formed. Nanofluids are engineered colloidal suspensions of nanoparticles within a base fluid. The nanoparticles may be produced from metal, metal oxides and different compounds. Metals such as aluminium, copper, titanium, boron, silver, etc. Different metal oxides like titanium oxide, aluminium oxide, silicon oxide, copper oxide, zirconium oxide, iron oxide etc. Different compounds like carbon nanotube, silicon carbide, calcium carbonate, aluminium nitride etc. were used to produce nanoparticles. The base fluid can also be changed for example, in place of water which is normally used, Engine oil, Glycerol can also be used. In recent technological advancement, heat transfer phenomena of Nanofluids are gaining attraction from researchers all over the world. Conventional heat transfer fluids are not sufficient for electronic devices because microprocessor being smaller and powerful, high heat transfer methodology is required to cool the microprocessor. A physical system contains particles of two different sizes, relatively small solvent molecules and somewhat larger nanoparticles with motion at two different time scales. The

nanoparticles are larger than the solvent (base fluid) molecules and consequently move much more slowly which can be computed by using Brownian dynamics simulation to effectively determine thermal conductivity of a nanofluid. [3] Heat transfer enhancement can be done by introducing Nanoparticles due to its high surface to volume ratio. The dispersed nanoparticles increase the surface area and the heat transfer capacity of the fluid. It avoids the problem of abrasion and clogging which is seen in case of large particles which reduces the usage of such kind of particles. With Nanoparticle inclusion, the interaction and collision among particles, fluid and the flow passage surface, mixing fluctuation and turbulence of the fluid are intensified. [4] Researching more on the thermal conductivity and heat transfer abilities of Nanofluids, it was found that carbon nanotubes average diameter of 30 nm, which were employed with volume concentrations of 0.001– 6% which generated elevated thermal conductivities. ($k_{\text{nanofluid}} < 3k_{\text{carrier fluid}}$) under static conditions. [5] But the quest for the capabilities of Nanofluids does not end here. Nanofluids are also widely used due to its improved properties that are relevant to engineering applications such as industrial cooling, extraction of geothermal power, automotive application like radiator coolant, lubricant etc., micro-scale fluidic application etc., and biomedical application as cancer therapeutics, nanosurgery etc. [6]

1.2.1 Surface Tension of Nanofluids:

The pull offered by a liquid when an object is taken out from it is known as surface tension. The tension between the surfaces can be understood with respect to the molecular interactions. Inside a liquid the molecules on average repel each other just enough to counter the pressure applied by the surroundings to the liquid. But again, the molecules at the surface are farther apart than the neutral distance. So, this surface tension is required if surface molecules are to be kept from moving from the surface into the bulk liquid. Over years many researches have been conducted on Newtonian as well as Non-Newtonian fluids. Hauner et al. [7] used pre-factor to determine the surface tension of water. The surface tension of water which is $\sim 72\text{mN/m}$ surprisingly showed surface tension is around $\sim 90\text{mN/m}$ which suggests the surface tension of a newly formed water surface is different from equilibrium surface tension, indicating of a surface relaxation that have taken place. The effect of addition of salt here increased the dynamic surface tension of water. Elevated values of about 80–100 mN/m for the surface tension of freshly formed water/air interfaces was

reported which relaxed to the equilibrium value within 1 ms. [8] Sibiriyakov [9] showed that at the room temperature surface tension drops as concentration increases. After critical concentration, called critical micelle concentration (CMS), tension reaches minimum and remain constant.

However, surface tension of the CTAB solution at 25 °C temperature is 37 mN/m and it slowly decreases with increase in the temperature. Then, at 60 °C, it begins to drop sharply from 33 mN/m to 27 mN/m at 75 °C, after which it slowly decreases again as shown in Fig. 1.2.1i which highlights on the fact that with surfactant in base fluid, the surface tension decreases which is also temperature dependent.

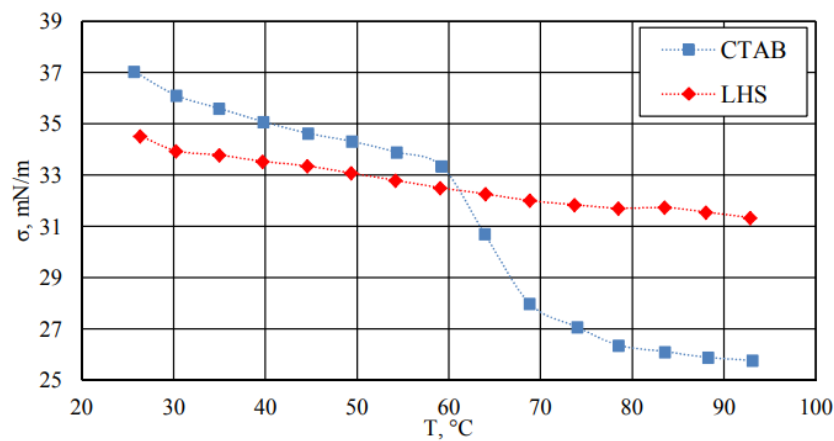


Fig. 1.2.1i Surface tension σ vs concentration C at 23 °C (Reprinted with permission from [9])

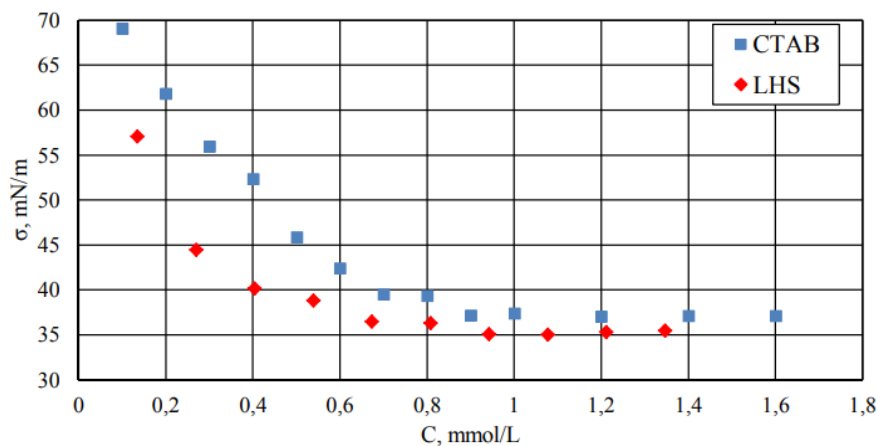


Fig. 1.2.1ii Surface tension of 1 mmol/L CTAB and 2.8 mmol/L LHS solutions vs temperature (Reprinted with permission from [9])

The concentration of the surfactant is equally important as shown in Fig. 1.2.1ii. The observation of higher measured surface tensions in microscopic droplets relative to the macroscopic solution is a consequence of the large surface-to-volume ratio of picolitre droplets as shown in Fig 1.2.1iii. [10] It is same for Nano-droplets as similar large surface-to-volume ratio characteristics is observed for the same. In a macroscopic solution, the fraction of surfactant molecules that partitions to the solution surface is negligible compared to the total number of molecules in the bulk because the surface-to-volume ratio is small and the total number of molecules in the solution volume is very large.

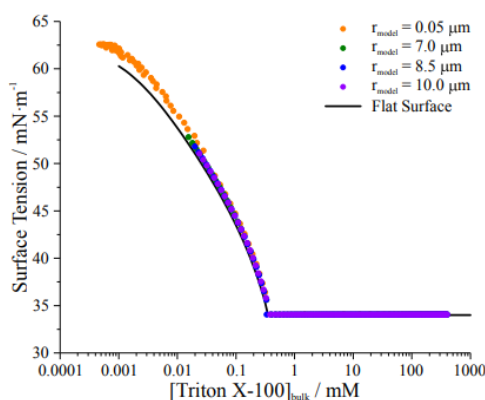


Fig. 1.2.1iii Monolayer partitioning of microscopic droplets
(Reprinted with permission from [10])

However, in a finite sized droplet, the fraction of surfactant molecules that partitions to the surface represents a significant portion of the total number of molecules in the droplet because of the large surface-to-volume ratio. [11]

Equilibrium partitioning of surfactant molecules to the surface of the micrometre radius droplet requires removal of a larger fraction of the total molecules from the bulk to form the surface film. A small increase in the absolute number of surfactant molecules in the droplet corresponds to a large increase in mole fraction of the surfactant, which can manifest as a sharp change in surface tension for small volumes. The key difference in the model is that the steep change in surface tension is due to size-dependent surface bulk partitioning, whereas in the 2D van der Waals model it is due to a phase transition in the surface film. [12] However, highlighting on the addition of surfactant in the base fluid, the interfacial tension increases or decreases with the increasing temperature. The addition of surfactants in base fluid

has a lot of importance in terms of oil recovery [13], food processing [14] and many more. Results have shown that interfacial tensions generally decrease with increasing surfactant concentrations and also with increasing temperature which is the general trend. However, an increase in interfacial tension with the temperature is sometimes reported for liquid/liquid systems containing species (surfactants, nano-particles, impurities) which are capable of adsorbing at the interface [15] [16] Yang et al [17] showed the effect of addition of anionic surfactant (Stepwet DF-95) on viscosity. Fig. 1.2.1iv shows that the solution viscosity decreases with the increase in the surfactant concentration and the solutions are shear-thinning. The increase in surfactant concentration results in the decrease in surface tension and then levels off at high surfactant concentrations.

For non-ionic surfactant (Alfonic 1412-3 Ethoxylate), with the increase in the concentration, the surface tension decreases much more rapidly as compared to other surfactants as shown in Fig. 1.2.1v. Alfonic 1412-3 Ethoxylate is more surface active than other surfactants.

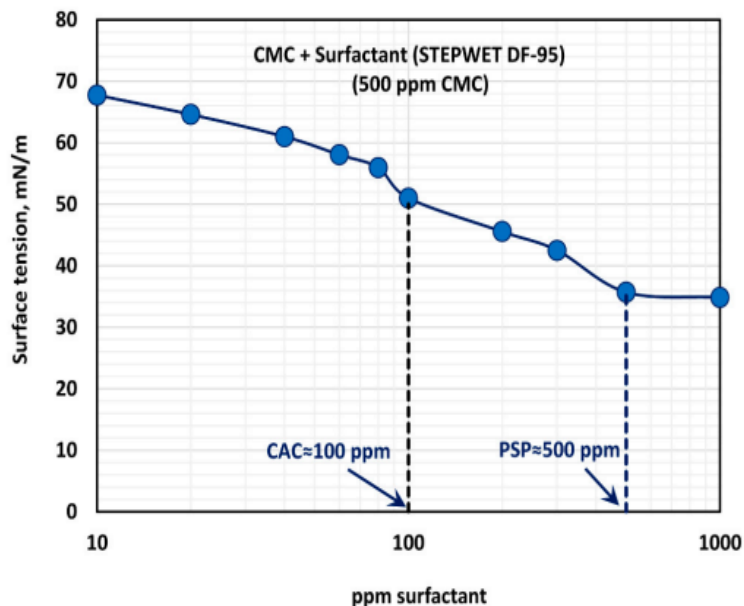


Fig. 1.2.1iv Variation of surface tension of surfactant-polymer solutions with the increase in surfactant concentration, at a fixed polymer concentration (Reprinted with permission from [17])

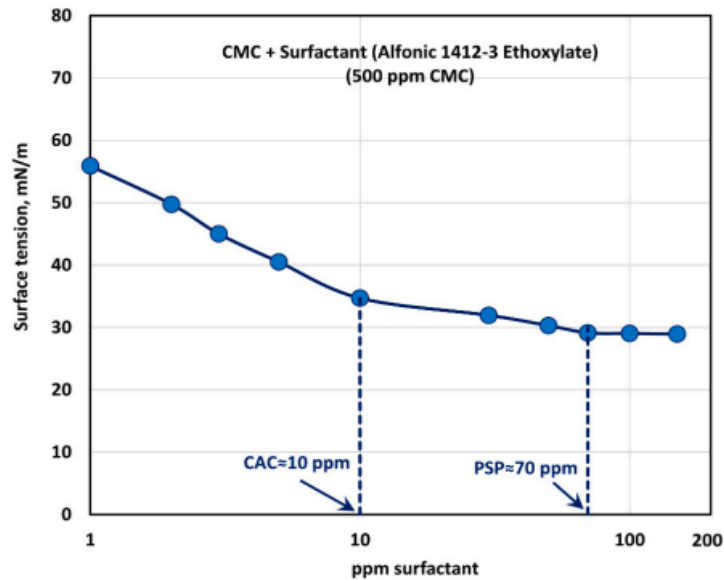


Fig. 1.2.1v Variation of surface tension of surfactant-polymer solutions with the increase in surfactant (Alfonic 1412-3 Ethoxylate) concentration, at a fixed polymer (CMC) concentration of 500 ppm (Reprinted with permission from [17])

While focusing on the benefits and characteristics of surfactants in various types of base fluids, the thermophysical properties of nanofluids are in recent studies. But the work on surface tension as well as viscosity is limited. Zhu et al [18] showed that higher solution temperatures result in lower surface tension. With the addition of nanoparticles, the surface tension increases linearly and then increase slowly. Similar kind of behaviour was seen with CNT-H₂O nanofluids. [19] Similar kind of trend was observed where the surface tension of CNT based nanofluids were higher than the base fluid. [20] Tanvir et al [21] showed that as the volume fraction of nanofluids increases with the addition of nanoparticles concurrently, the surface tension increases as well. This is because of the cohesive force which acts as the nanoparticles are driven closer to the base fluid. An attractive Van der Waals force is employed over the electrostatic repulsion force between the molecules which further increases the surface tension of the nanofluids. Fig. 1.2.1vi shows the dependency of surface tension on concentration of nanoparticles of various sizes and compounds. [22]

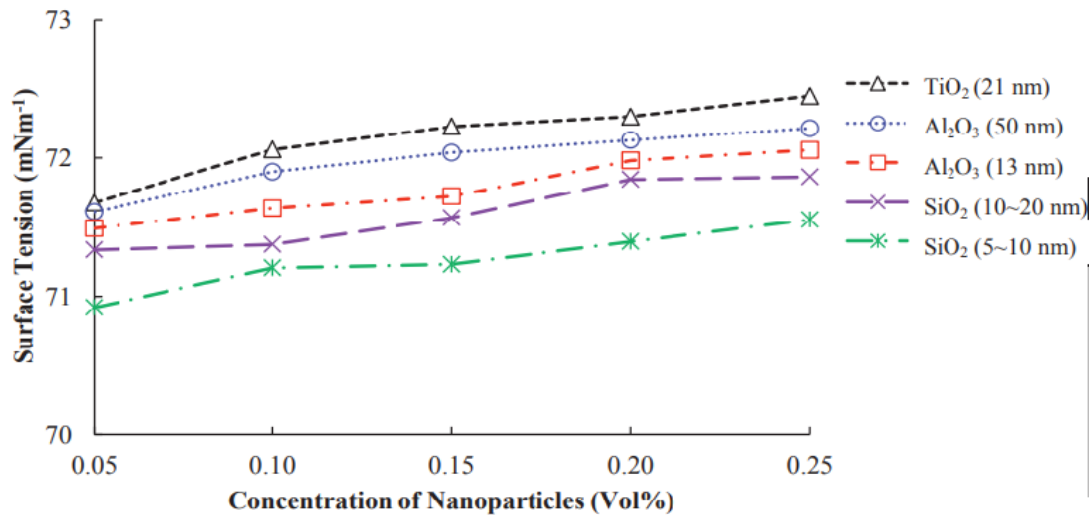


Fig. 1.2.1vi Surface tension of nanofluids as a function of volume concentration at 25°C (Reprinted with permission from [22])

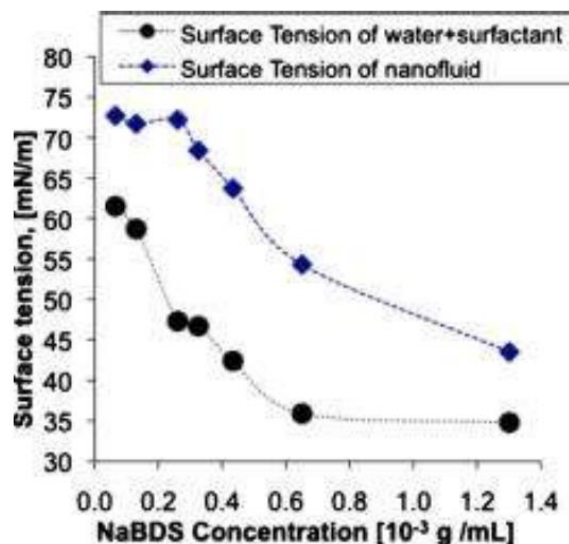


Fig. 1.2.1vii Surface tension of DI water+NaBDS and surface tension of p-SWNTs nanofluid with NaBDS (Reprinted with permission from [23])

However, a different kind of result is obtained when we measure the surface tension of nanofluids plus surfactant as shown in Fig. 1.2.1vii. The mixing of SWNTs/Water nanofluid with NaBDS surfactant shows that surface tension initially decreased and then gradually and becomes constant. The decrease was due to the fact that most of the surfactant molecule was mixed with DI water. [23]

In some cases, an initial decrease in surface tension was observed for nanoparticles up to 0.5% and remains almost constant up to 2–3 wt.%. After that, the surface tension of nanofluid

increases with increasing particle concentration. At low particle concentrations, the trends are different for various base fluids, particles, with or without a surfactant. [24]

Murshed et al. [25] on testing TiO_2 /Water nanofluids with surface tensiometer found that the surface tension of the resulting nanofluid decreases at room temperature from that of water. With sessile drop method, Bi_2Te_3 /water nanofluid showed a decreasing surface tension trend with increasing particle concentration until it reaches a minimum and then increase with increasing particle concentration. [26] It is believed that accumulation of nanoparticles at the gas-liquid interface to be responsible for the surface tension behaviour. There are certain surfactants which does not affect the surface tension of nanofluid like PVP (polyvinylpyrrolidone). [27] Fig. 1.2.1viii shows one of the trends where surface tension of nanofluids show curvy behaviour. This happens because of the Van der Waals force created due to the nanoparticle and surfactant and a specific kind of flow pattern which is yet to be explained. In some cases, the presence of nanoparticles in surfacted liquids shows two competing effect. One which shows the nanoparticles adsorb the surfactant, leading to an increase in the interfacial tension. In other context, the nanoparticles tend to attach themselves to the interface, thereby reducing the overall interfacial tension. [28]

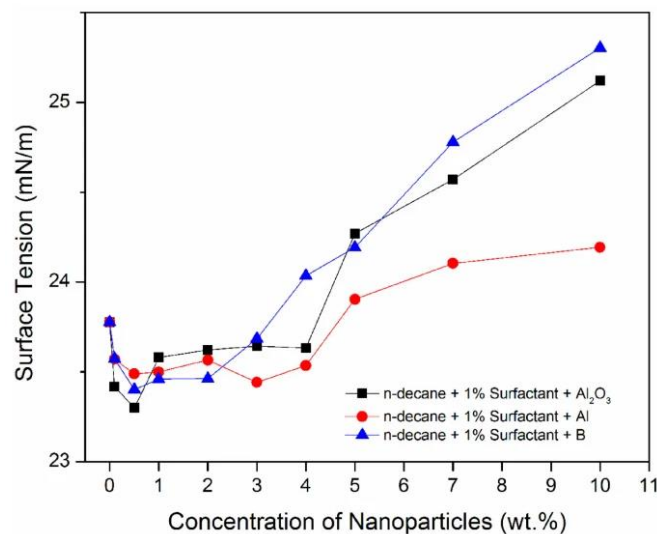


Fig. 1.2.1viii Surface tension variation with nanoparticle concentration for n-decane based nanofluids (Reprinted with permission from [28])

However, Das et al [29] showed that Surface tension of nanofluids increases with increase in solid volume fraction and decrease with temperature. AA-stabilized nanofluid showed significantly higher surface tension compared to that by CTAB stabilized nanofluid.

1.3 Literature review:

This section discusses some of the salient literatures that has been investigated regarding impingement of Nanofluid droplets on super-hydrophobic surfaces. But a comparison should be drawn on how only base fluids behave when it is impinged over super-hydrophobic surfaces.

Droplet impact on solid surfaces, practically can be seen around us. For example, rain, steam cooling or fog formation. However, due to its impactful applications such as Spray cooling, Ink-jet printing, pesticide painting, researchers around the world are excited about it's positive outcomes that will benefit human life. The effect of Weber Number, surface roughness and fluid type, determines the spreading, recoiling, oscillating and splashing of the droplet. Both experimental and theoretical insights were presented in this work. The type of nanoparticle, the base fluid, the preparation methods were elucidated in this work. The findings from this work involve normalised drop height, normalised drop radius and its variation with respect to concentration of Nanoparticles, impact of super-hydrophobic as well as super-hydrophilic nanoparticles, the contact line pinning effect. The method of cooling is capable of providing higher heat transfer coefficient such as impinging jets [30]. The conclusion which was drawn was based on the fact that hydrophobic nanoparticles can significantly alter the dynamics of droplet impacts, while hydrophilic particles showed little effect on the droplet dynamics. Kahani et al. [31] showed that the colloidal dispersion of TiO₂ nanoparticles in water droplets improved the heat transfer on uncoated and superhydrophobic surfaces over that of pure water. No significant trends were observed on superhydrophilic surface. However, poor wettability of the surface can reduce cooling energy. The pinning effect generated by the hydrophobic nanoparticles is a function of the Weber number of the droplet and hydrophobic particle concentration. In low particle concentration, the critical Weber number is used to represent the transition from no-pinning to pinning which is negatively correlated with the hydrophobic particle mass fraction.

- Nanoparticle chosen: Commercial hydrophilic SiO₂ nanoparticles, Hydrophobic SiO₂ nanoparticles.
- Base fluid: Mixture of deionized water and ethanol. (Ethanol volume concentration at 5%)
- To ensure the stability of Nanofluids, Malvern laser particle analyser was used to examine zeta potential and the diameter distribution of the nanoparticle.

- Average initial droplet diameter (D_0) $\sim 2.08\text{mm}$
- To measure surface tension and contact angles, contact angle meter was employed.
- To study the rheological behaviour, rheometer was used.
- To study the size and morphology of the samples, TEM and FESEM were used.
- In the analysis below, Hydrophilic SiO_2 and Hydrophobic SiO_2 were used as materials for Nanoparticles which is to be mixed in a base fluid for making Nanofluids. The mass concentration and velocities were 0.01-0.5 wt% and 0.5-2.0 m/s respectively. Fig 1.3i shows the droplet dynamics on impingement over the surface.

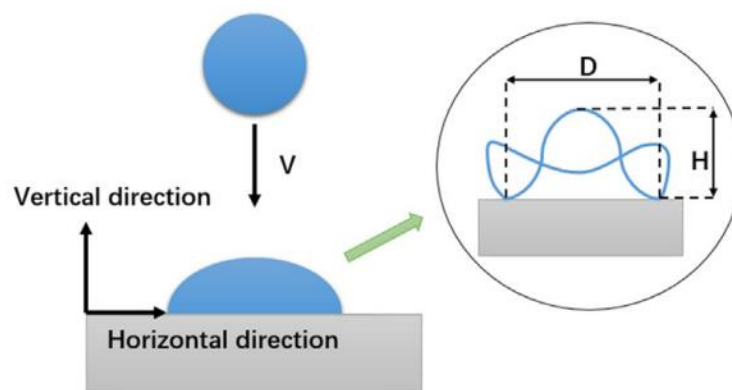


Fig. 1.3i Droplet dynamics illustration (Reprinted with permission from [32])

1.3.1 Effect of Hydrophilic Nanoparticles on Droplet impingement:

The average particle diameter of suspensions is independent of particle concentration, regardless of hydrophilic particles or hydrophobic particles. It was found that hydrophobic particles had a greater tendency to agglomerate in the base fluid than that of hydrophilic particles.

To analyse the impact dynamics of droplets, normalised drop height (H/D_0) and normalised drop radius (D/D_0) on Hydrophilic as well as Hydrophobic surfaces were examined. [32]

Once the hydrophilic particle laden droplet impinges on the surface, there are stages which it undergoes:

- At $t=1\text{ms}$, the velocity perpendicular to the surface is redistributed to velocity parallel to the surface. That means the droplets spread radially outward and increase their surface area and also surface energy.
- At $t=6\text{ms}$, the spreading velocity decreases to zero with minimum thickness and maximum radius. The shape starts taking a pancake with a dominating surface tension force which causes retraction.
- At $t=24\text{ms}$, the droplets retract and rebound to their maximum height and enters a damped oscillation stage.
- At $t=80\text{ms}$, the damped oscillation gradually weakens with irreversible dissipation of kinetic energy, and the droplet finally reaches a stable state.
- Here the locking between the surface and the droplet is seen to be dominating. The amplitude of damped oscillation of the droplet in the vertical direction was stronger than that in the horizontal direction.

Semenov et al. explained this phenomenon in a similar way [33] which proves that irrespective of the type of fluids, the events are same in all the cases.

Droplet containing hydrophilic nanoparticles with higher viscosity does not show higher pinning effect. This means increase in viscosity is not the only reason why the hydrophobic nanoparticles show changed impact dynamics. Investigation was also done on the effects of particle structure formation and the structural disjoining pressure of nanoparticles on the spreading of nanofluids on solid surface. The findings showed that the in-layer particle structuring can optimise and enhance spreading of nanofluids on solids. [34] Robert et al. [35] compared the impingement of water and Nanofluid. It showed that the initial dynamics of nanofluids is similar to that of water. The droplet impinged on top of the silicon surface leads to the decrease in surface temperature on the circular area on the bottom face of the wafer. The cooled area increases in diameter over time, but its growth rate decreases as the droplet spreading velocity decreases. The area affected by the nanofluid droplet is larger than the size of the area affected by the water droplet. The size of the area affected and amount of temperature change. The nanofluid droplet impinging on the superhydrophobic surface does not have as much surface tension like water droplet, and does not rebound strongly.

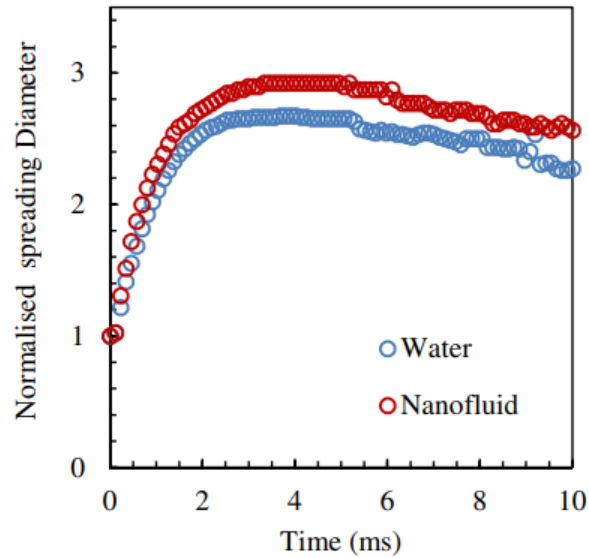


Fig. 1.3ii Normalised droplet diameter over time for water and 0.5% w/w concentration nanofluid droplets impinging onto an uncoated surface (Reprinted with permission from [34])

The surface contact angle influences the maximum spreading diameter of the droplet, contact time and effectiveness of heat transfer as shown in Fig. 1.3iii. The influence of the nanoparticle laden droplets results in increase in increased pancake diameter with reason might be the Marangoni effect or is yet to be investigated. For single droplet impingement events, it was observed that hydrophilic surfaces (contact angle $< 25^\circ$) offer a higher cooling effectiveness than both uncoated (contact angle $\sim 90^\circ$) and superhydrophobic surfaces (contact angle $> 160^\circ$). If this is also true for a nanofluid, then it will provide an additional means by which heat transfer can be enhanced. [36]

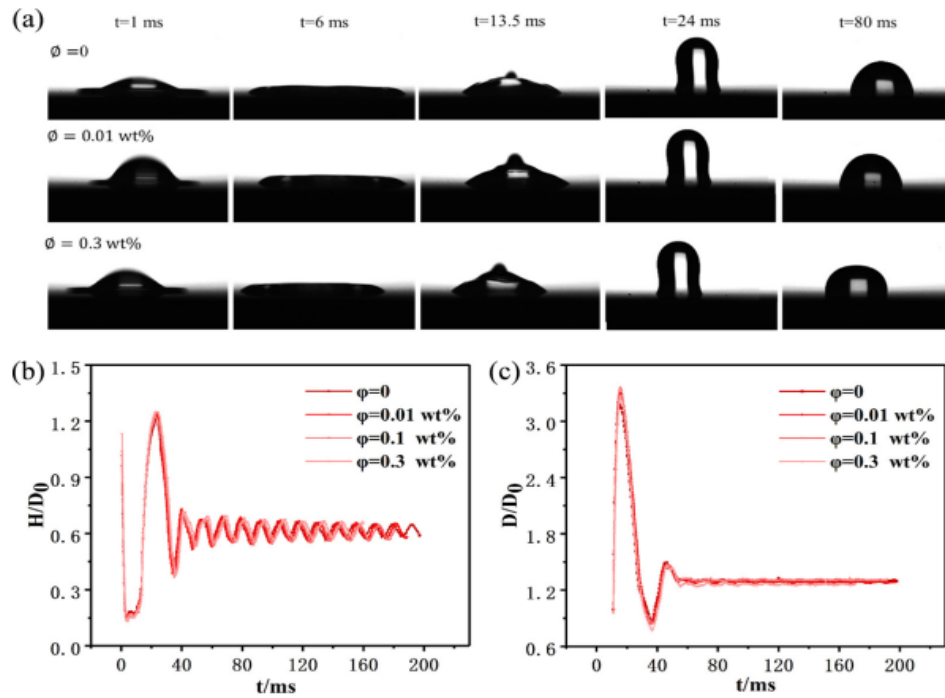


Fig. 1.3iii Evolution of droplets containing hydrophilic SiO₂ particles after impacting on a solid surface (a) Evolution images of droplets (b) Dimensionless height of spreading drops, H/D_0 (c) Dimensionless radius of spreading drops, D/D_0 (Reprinted with permission from [32])

As the wetting transition approaches, the contact angle decreases and becomes equal to zero at and above wetting transition which proves the nature of hydrophilicity. But in order to examine the line tension, the microscopic surface structure and surface interactions in three phase contact line. Fig. 1.3iv shows the impact characteristics for base fluid and nanofluid which clearly shows that there is a regime jump for D/D_0 curve over time. For the above stated reason, locking effect at the interface between surface and nanoparticle laden droplet dominated which limited the motion of the droplet in radial direction. [37]

However, for shear thinning droplets like nanofluids, majority of focus is on maximum spreading of shear thinning of the drop. The shear thinning fluid is the one where viscosity decreases as the shear rate increases whereas the viscosity of a Newtonian fluid remains constant regardless of the shear rate. However, two kind of Newtonian plateaus are noticed for viscosity curve of shear thinning fluid. One is extremely low shear rate and extremely high shear rate. [38]

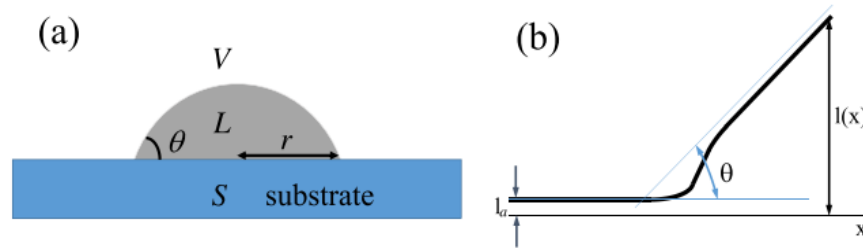


Fig. 1.3iv (a) Liquid droplet of lateral radius r and contact angle θ at a substrate – vapor surface (b) In the immediate vicinity of the three-phase SLV contact line, the liquid thickness $l(x)$ varies with distance x along the substrate (Reprinted with permission from [37])

1.3.2 Effect of Hydrophobic Nanoparticles on Droplet impingement:

In another experiment, hydrophobic SiO_2 nanoparticles were considered. Certain changes in droplet dynamics were observed in this case:

- With particle concentration of 0.01 wt.%, the evolution of droplet containing such particles after impinging on solid surface coincide with the base fluid.
- With increase in particle concentration, the contact line pinning and receding breakup phenomena occurred in retraction stage.
- During the receding breakup, the liquid at the edge shows retraction lag while the liquid at the middle contracts rapidly which resulted in some part of liquid being left by the receding droplet.
- The above phenomena varied with particle loading. For 0.1 wt.%, the phenomenon was weaker. It improved slightly for 0.3 wt.% and for 0.5 wt.%, the droplets were directly nailed to the solid surface.
- Surprisingly, the maximum spreading radius was independent of the particle loading whereas the retraction height decreases with increased concentration. But the dimensionless radius of the spreading droplet decreases once the concentration increases above 0.1 wt.%. This can be explained with pinning effect at the contact line. This is the reason why the diameter of the droplets remained almost stable even after 12 ms.

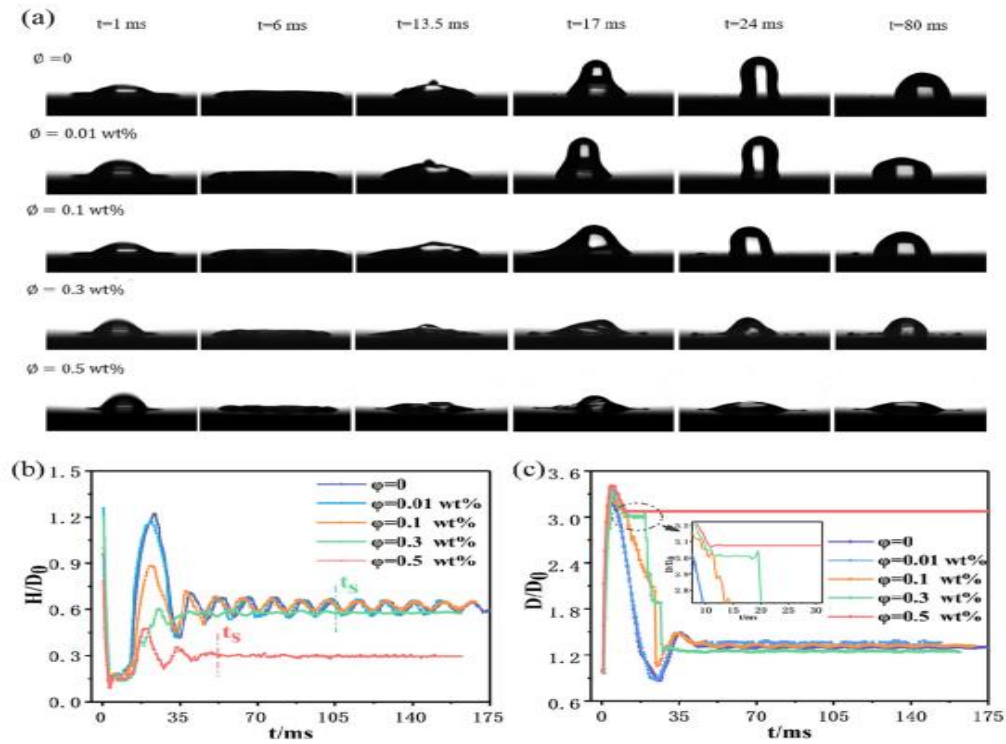


Fig. 1.3v Evolution of droplets containing hydrophobic SiO₂ particles after impacting on a solid surface (a) Evolution images of drops (b) Dimensionless height of spreading drops, H/D_0 (c) Dimensionless radius of spreading drops, D/D_0 (Reprinted with permission from [32])

As shown in Fig. 1.3vi, it is seen that as the particle loading exceeds 0.3wt%, the damped oscillation response time of the droplets in vertical direction decreases. When it is less than that, it took 200 ms more to come to steady state. However, when the particle loading was increased to 0.5 wt.%, the response time was reduced to 52 ms. So, the hydrophobic particle concentration was responsible for reducing the response time for hitting the solid surface by more than 75% for higher concentration. This phenomenon attributes the increased droplet dissipation energy due to droplet dissipation energy. Talking about nanofluids, it gives uniform spreading characteristics than any other fluid. [39]

For the same impact velocity cases, the contact line pinning effect can reduce maximum droplet retraction height from 1.2 to less than 0.9 which shows that the energy consumption due to pinning is significantly large. However, the contact line pinning depends upon droplet retraction time, contact area and fluid viscosity.

The suspensions containing hydrophobic particles had an increased viscous dissipation due to the effect of increased viscosity and as a result moving line dissipation.

So, the maximum retraction height and relaxation time were reduced. Due to high impact velocity, the droplet spread initially increased. Due to the high shear rate, the hydrophobic particles showed low viscosity and so maximum spreading diameter was not affected by the particle concentration while spreading phenomena. [40] But in general, the increased hydrophobic particle concentration increases the viscosity of the nanofluid such that the local viscosity near the droplet three-phase line would significantly increase.

Hydrophobic nanoparticles in base solution are more likely to adsorb and deposit on three-phase contact line, forming a viscoelastic film as compared to hydrophilic nanoparticles which are dispersed uniformly in base solution. The increased concentration of hydrophobic particles will increase the viscosity of suspensions and base fluid in shear stable state, allowing local viscosity near three phase contact line to increase. It is because of the adsorption and deposition near the contact line which increases the surface roughness. The surface roughness however has a positive effect on the friction force and excessive dissipation near the contact line. The maximum spreading radius remains unaffected because of the lower viscosity caused by the higher spreading speed in the initial stage of the impact. Fig. 1.3viii shows the dependency of viscosity over shear rate. No such dependency is seen in this case. The reason of anomaly in case of hydrophilic nanoparticle is that the nanoparticles gets entrapped between the intermolecular spacing of the base fluid. As a result, no such shear rate variation is seen for hydrophilic nanoparticles. Whereas for hydrophobic nanoparticles, there is a relationship between the viscosity and shear rate. The reason been the hydrophobicity of the particles which creates a collision with the base fluid molecules.

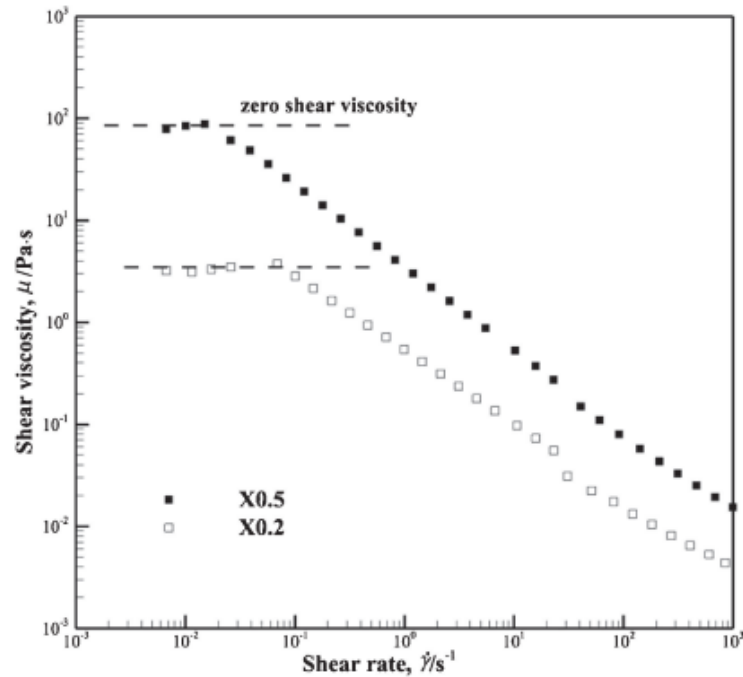


Fig. 1.3vi Measured shear viscosity with respect to shear rate (Reprinted with permission from [41])

The effect of hydrophilic nanoparticles resulted in the behaviour of Newtonian fluid. Fig. 1.3vii shows that viscosity is independent of the shear rate like the water. The suspensions containing hydrophobic nanoparticles exhibits shear thinning behaviour indicates that the viscosity of the suspensions decreased rapidly with increased shear rate showing stronger agglomeration tendencies in base solution than hydrophilic particle. [41]

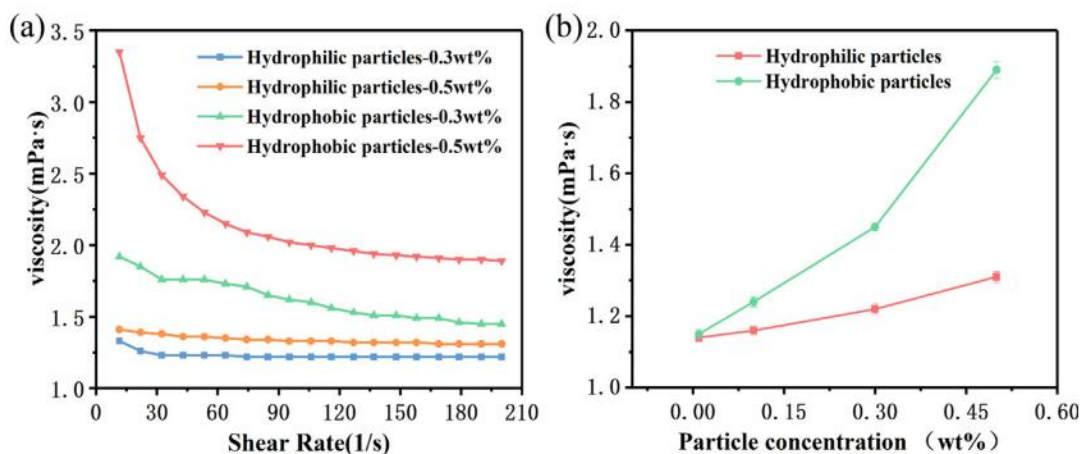


Fig. 1.3vii (a) Variation in viscosity with shear rate of SiO₂ suspensions (b) Variation in viscosity with particle concentration in shear steady state (Reprinted with permission from [32])

The hydrophobic particles tend to be distributed on the droplet surface in chain or in a network near three phase contact line forming a visco-elastic film over the surface. Such particles exhibit preferential absorption on three phase which results in increase in the concentration and surface roughness near the contact line. [42]

1.3.3 Friction Energy Dissipation due to particle rebound:

During the contact line advancing and receding phase, energy is dissipated by three ways. Line dissipation, viscous dissipation and friction around the contact line. Snoeijer et al. [43] showed that when the contact line moves with respect to the substrate the system is no longer at equilibrium. The hydrodynamics is in essence described by a corner flow which has no intrinsic length scale [44]. Lack of intrinsic length scale of the flow means that only a local Reynolds number based on the distance to the contact line can be defined. As the distance can become arbitrarily small, the Reynolds number is typically very small, and inertia can often be neglected. The rate of energy dissipation E' (per unit contact line), which between a distance r and $r + dr$ scales as

$$dE \sim \eta u^2 (dr/r) \sim \eta u^2 (d \ln r) \dots\dots\dots(1) \quad [45]$$

The above equation implies that total dissipation which cannot be integrated at $r = 0$ nor at ∞ , and one requires a cut-off at both small and large scales. The cut-offs appear at the molecular scale.

In other instance, the dissipation effect caused by friction near the contact line states that there is a friction associated with the displacement of molecules around the contact line and the friction force is linearly dependent on the velocity at lower velocities [46]. Reducing viscosity affects the droplet dynamics and likewise decrease in power dissipation. At small and intermediate droplet velocities, there is an excess dissipation which cannot be accounted for the viscous effect of the droplet. So, a linear contact line model was introduced to represent the excess dissipation in small and intermediate velocity.

$$F = \xi U \dots\dots\dots(2)$$

where ξ = contact line friction coefficient (dynes s/cm²) [47]

The above equation can explain the phenomena of increased surface roughness which promotes the friction force near contact line. So, both friction resistance and local viscosity near the contact line should be the reason for contact line pinning. However, a number of factors influence the particle rebound like addition of polymer additives. The droplet rebound will be suppressed by such additives. It is due to the increase in elongation viscosity. [48] In this case the energy dissipation is significantly high, due to more friction in the contact line. The so called elongational or extensional viscosity remains a problem in non-Newtonian fluid like nanofluids [49]. On the other hand, energy transfer can be understood by Ohnesorge number which is the ratio of viscous force to inertial force and surface tension force. [50]

Theoretically, the absorbed heat travels through the droplet faster than it would do in pure water and absorbing its full thermal energy faster. This means greater energy is absorbed by nanofluid for a very short impingement duration because of a quicker distribution throughout the droplet. [51]

The energy generated from the impact is transferred through capillary waves along the air–liquid free surface and the liquid viscosity obstructs the transfer of energy. There are some data which provide evidence that at high Oh values, viscous damping weakens the capillary waves, possibly resulting in a reduction of the mass transport. [52]

1.3.4 Effect on Weber Number:

The impact velocity is the factor which determines the dynamics of droplet over the surface. The overall drop impact process over the surface is characterized by Weber number which is the ratio of kinetic energy and surface energy.

$$We = \rho V^2 D / \sigma \dots \dots \dots (3)$$

where ρ = Density of the fluid

V = Impact velocity

D = Initial diameter of the droplet

σ = Surface energy

In a particular study [53], neither pinning nor receding breakup phenomena was observed for Weber number 8.5. The thickness of the liquid film is thick and pancake diameter is small. The particles absorbed near the contact line can be brought back easily by the retracting liquid as the friction and local viscosity near the contact lines

are weaker. As the Weber number increases, the pinning effect increases and at Weber number of 16.7, the pinning begins to appear which leads to plenty of energy dissipation with a much smaller recoil height. A directional movement of droplet was found between 16.7 to 34.0.

As shown in Fig. 1.3ix, with the increase in impact velocity, the droplets achieve maximum retraction due to increased velocity and inertial energy. So, the receding breakup phenomena was observed at the Weber number of 76.6 and the normalised spreading radius increased with the increase in Weber number.

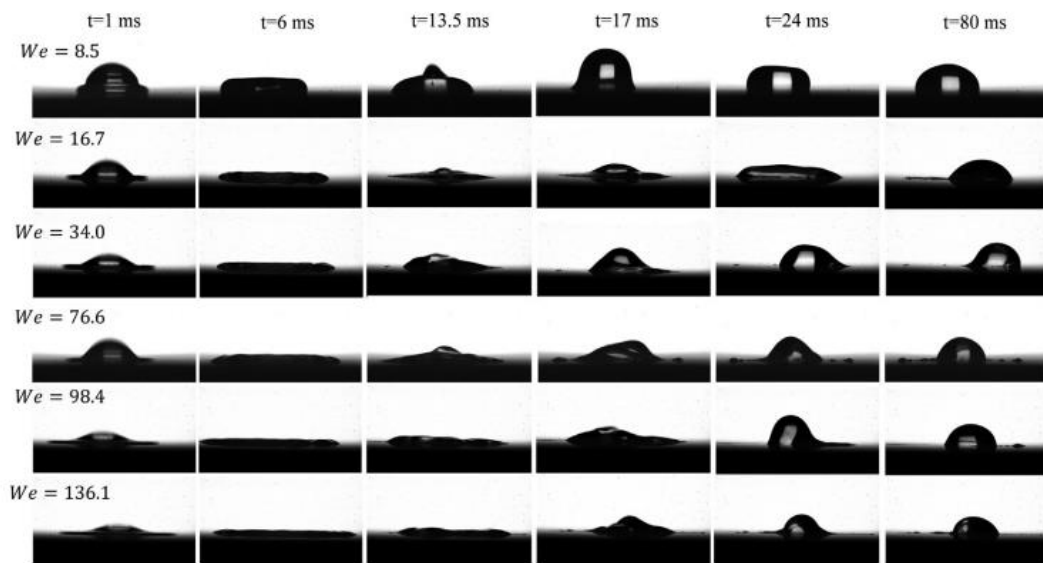


Fig. 1.3viii The evolution of droplets containing hydrophobic SiO₂ particles at a concentration of 0.3 wt% post-impact on a solid surface under different Weber number (Reprinted with permission from [32])

Experimentally, normalised maximum recoiling height decreases rapidly as the Weber number increases and then it increases with increasing impact velocity. However, the normalised spreading radius increases with increase in Weber number. For lower Weber number as low as 0.3, it was seen that the droplet was deformed after impacting on the CNT array surface and then slight drop expansion and recoiling as well as oscillation around its equilibrium position in the vertical direction occurred till its kinetic energy was totally dissipated by liquid viscosity. The nano-sized topography ensured CNT arrays to maintain the Cassie state superhydrophobicity. [54] However, during the receding phase, the air bubble entrapment was often observed and the difference in receding velocity between the

top and bottom parts of the droplet accounts for such air bubble trapping phenomena which is the main cause of such low Weber number [55]. However, at a slightly greater Weber number, droplet deformation occurs. The droplet rebound process at a slightly greater Weber number usually results in stretched neck and which results in breakage and formation of satellite droplets owing to Rayleigh-Plateau instability [56]. The formation of satellite droplets at the crown top is attributed to the theory of capillary instability of free rim and bending perturbations of the toroidal rim [57]. This phenomenon largely occurs due to increased Weber number.

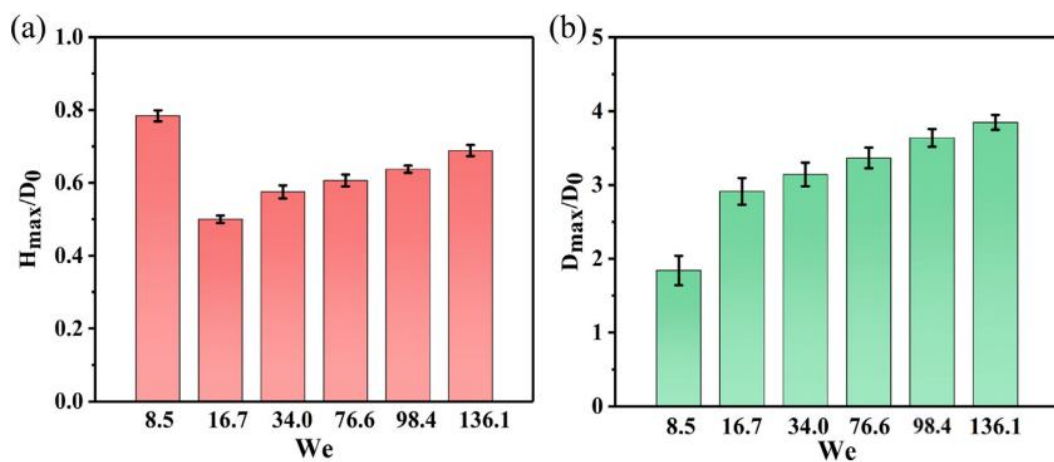


Fig. 1.3ix (a) Dimensionless maximum recoiling height (H_{\max}/D_0) (b) Dimensionless maximum spreading radius (D_{\max}/D_0) for droplets with hydrophobic particles at a concentration of 0.3 wt% (Reprinted with permission from [32])

1.3.5 Pinning effect due to nanoparticles:

The contact line pinning should be the function of Weber number and hydrophobic particle concentration. Fig. 1.3xi shows the critical Weber number which is used to represent the region from no pinning to pinning fitted as a function of mass fraction of hydrophobic particles. The critical Weber number decreased rapidly with increase in hydrophobic particle concentration at lower particle concentration and it disappears once the concentration reaches 0.5wt%.

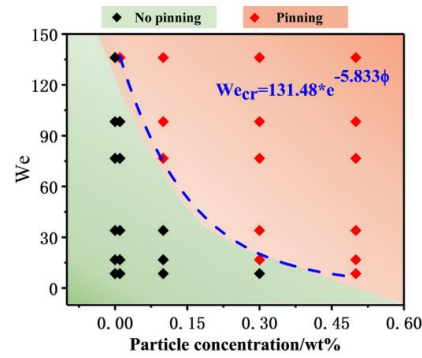


Fig. 1.3x Regime map for contact line pinning as a function of the Weber number and hydrophobic particle concentration (Reprinted with permission from [32])

Dengwei Jing et al. [58] showed that as the impact velocity continues to grow, the pinning is weakened. Without the contact line pinning, the maximum rebound height of the droplet is still smaller than that of the water droplet. For the concentration greater than 0.1 wt%, the pinning emerges in the range of 253–351. The results indicate that the inertia of particles play a crucial role in the occurrence of the pinning phenomenon.

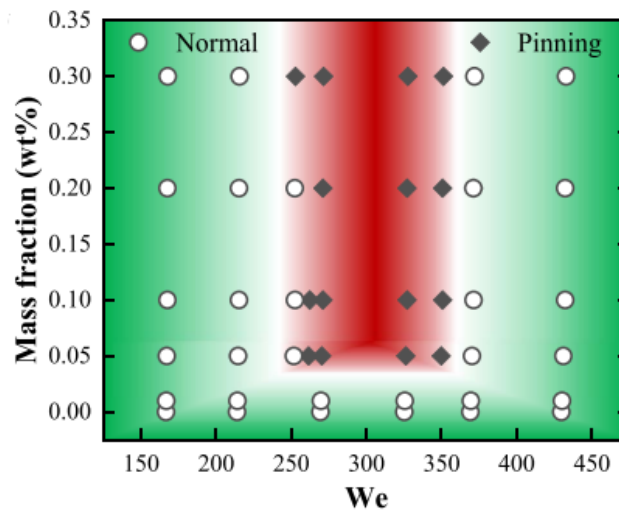


Fig. 1.3xi Regime map for whole contact line pinning as a function of the Weber number. The normal situation means the contact line retracts immediately. (Reprinted with permission from [32])

The pinning effect affects the Weber number. Under the condition of low Weber number, thick liquid film and small spreading diameter, the increased friction and local viscosity near the contact line are weaker than the droplet retraction inertia force.

$$F_k > F_{\text{viscous}} + F_f \dots\dots\dots (4)$$

where, F_k = retracting inertia force.

F_{viscous} = Viscous resistance.

F_f = contact line friction force.

However, with the increase in impact dynamics, the spreading diameter increases which results in increase in contact line dissipation and viscous dissipation, thus reducing the available energy for retraction. For this reason, the retraction inertia force decreases, while the surface friction force and viscous resistance increase due to the absorption of more hydrophobic particles near the contact line causing a pinning effect to appear in droplet retraction process as shown in Fig. 1.3xiii.

$$F_k < F_{\text{viscous}} + F_f \dots\dots\dots (5)$$

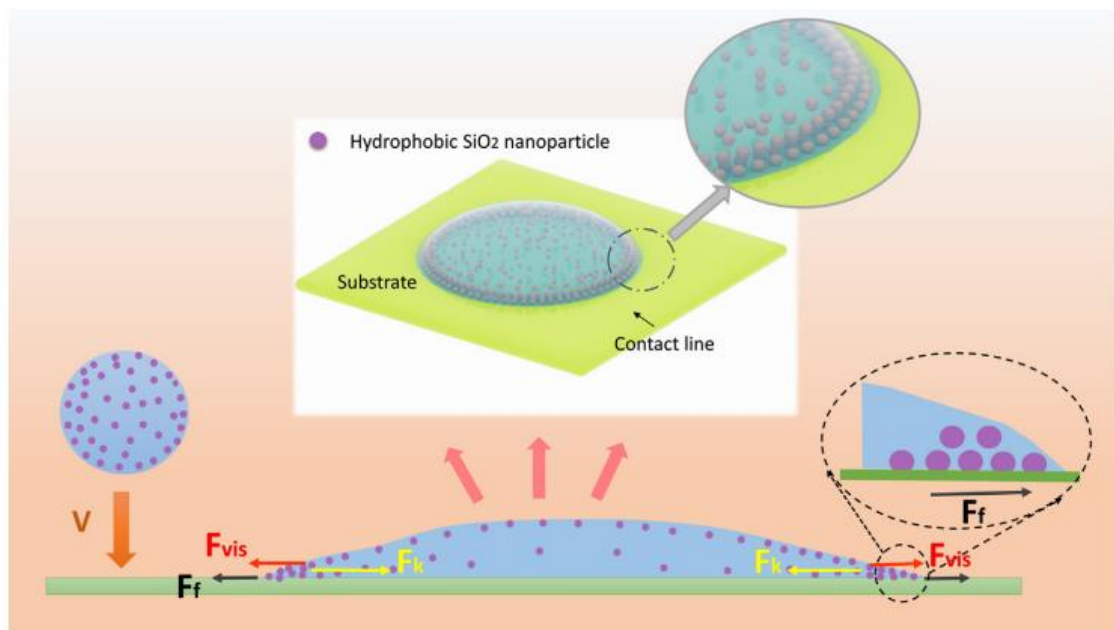


Fig. 1.3xii Schematic illustration of the effect of hydrophobic nanoparticles on the dynamics of droplet impacts. F_k is the retracting inertia force, F_{viscous} is the viscous resistance and F_f is the contact line friction force. (Reprinted with permission from [32])

The droplets remain directly nailed to the solid surface retraction resistance and the inertial force are balanced.

$$F_k = F_{\text{viscous}} + F_f \dots\dots\dots (6)$$

The liquid at the edge of contact line can produce a contract lag due to the pinning effect while the liquid at the middle contracts rapidly, resulting, a part of the liquid being left behind by the receding droplet, a phenomenon that is called receding breakup phenomenon, the way that can destroy the pinning effect. So, during receding droplet breakup needs to dissipate energy, and the broken and detained liquid will also directly take away parts of the droplet energy. Sefiane et al. [59] concluded about impinging effect which could be reasoned as higher substrate temperatures and after depinning the contact angle remains far from the initial one. Depinning occurs when the corresponding contact angle reaches a minimum critical angle. So, it is not necessarily always be the effect of the nanoparticles but the temperature

Another effect which can be taken into consideration is variation of friction between droplet and substrate by sliding angle.

1.4 Gap Area:

Lot of experiments were performed related to the impact dynamics of Non-Newtonian fluid as nanofluids, but very few experiments were carried out on the impact behaviours and dynamics of the nanofluids on engineered surfaces. Not only that, there are less report on the impact behaviour of nanofluids with surfactant along with the change in particle concentration as well as droplet size, which is the main aim of the thesis. However, progression in research regarding the formation of satellite droplets at a particular Weber number has rarely been reported. Li et al. [60] reported the change in dynamic spreading behaviour with the increase in nanoparticle volume fraction which directly relates with the viscosity effect. But observations relating to nanofluid impact along with varied concentration of surfactant and droplet diameter and the critical Weber number for which crowning and critical Weber number for splashing occurs has been not been reported. The present thesis reflects these aspects.

1.5 Objectives:

The objectives of current experiments were:

- Preparation of TiO₂-Water Nanofluids with CTAB surfactant in the ratio 1:10 in volume fractions 0.01%, 0.1% and 0.5% volume fraction using bath sonicator.
- Preparation of Superhydrophobic surfaces.
- To analyse the pancake diameter of the droplet after impingement on superhydrophobic surface and analyse the spreading and receding pattern.
- To analyse the varying effect of droplet diameter and its impact on Droplet spreading on superhydrophobic surfaces with varying height.
 - To analyse the variation of pancake diameter with Weber Number.
 - To analyse the variation of Spread factor with Weber Number.

Chapter 2

2. Materials and Methods:

2.1 List of Equipment and Materials Used:

2.1.1 Equipment used:

- High Accuracy Electric Weight Balance Machine (Sartorius, BSA 224S – CW, max 220g, accuracy 0.1mg)
- Bath Sonicator – (Model – USB 3.5L H DTC, Serial No. – 369 APR 2017, Supply volt – 230V AC 50Hz)
- Magnetic stirrer – (REMI, 2MLH)
- Magnetic stirrer rods - The small one (3cm length)
- Measuring cylinder – Borosilicate Glass
- Lab glass bottles – Borosilicate Glass
- Wash Bottle
- Medical syringe – Dispovan medical syringes
- Blue needle- 0.714mm
- Yellow needle-0.231mm
- Dispovan medical syringe needle (Purple needle-0.540mm)
- Vision research AMTEK Phantom highspeed camera (Model- VEO 310L)
- Pro Series Auto Focus Macro extension tube set (12mm,20mm,36mm)
- Nikon AF NIKKOR 50mm 1:14D camera lens
- Manfrotto 055 Tripod for camera mounting.
- GS VITEC LED Lamp (Model- MultiLED LT, Power supply- 24V 150W)
- Optical Bench

- Optical bench rail
- Fisher clamp
- Retort stand

2.1.2 **Materials used:**

- TiO₂ Nanoparticles (Sigma Aldrich) of average size in diameter 21 nm.
- Distilled Water (Merck Millipore) with purity 99.7%
- Surfactant – Cetyltrimethylammonium Bromide (CTAB), (SRL) Extra pure AR, Powder Form, 99% purity.
- Acetone (Fisher Scientific) CAS No.: 67 – 64 – 1, (CH₃)₂CO = 58.08, Prod. No.: 3351C, 99% purity.
- Iso-Propyl Alcohol
- Aluminium plate
- Sandpaper

2.2 **Fabrication of Superhydrophobic surface:**

Various scientists have developed processes for the fabrication of superhydrophobic surfaces. This kind of surfaces are of great importance in applications such as self-cleaning for vehicle windshields, display panels etc. The contact angle hysteresis for this kind of surfaces is larger than 5° but apparently the contact angle is larger than 150°. However, it is not easy to obtain low contact angle hysteresis for surfaces with low contact angles. [61] Shang et al. [62] created four different surfaces which involves a smooth surface achieved by dip-coating sol–gel films, an assembly of uniformly sized spherical nanoparticles, a uniformly sized nanorod array unidirectionally aligned perpendicular to surface and an open mesh of nanofibers lying parallel on a substrate.

A nanoparticle film was made from a mixture of TEOS and ethanol with NH₄OH (30% in water) as a catalyst. At the beginning, 3ml of NH₄OH was added into 50 ml of ethanol and stirred at 60°C for 30 minutes after which 3 ml of TEOS was added dropwise. After 90 min of stirring the final sol B was obtained which consist of monosized spherical silica nanoparticles approximately 100 nm in diameter. [63] However, the method

employed here is different as compared to the literatures. Here multiple stages are involved.

- An Aluminium surface is considered with a plain top. Initially, a sand paper is taken to peel off the topmost layer and make the surface rough.
- The next step involves treatment of the surface with Acetone in a bath sonicator for 15 minutes to disperse off the particles from the top layer.
- After the treatment with Acetone, treat the surface with normal water in a bath sonicator for 15 minutes.
- The next step involves etching off the top layer of the surface with 3M HCL. The rate of reaction is initially quick but over time the reaction slows down indicating that the rough part over the surface is peeled off and a smoothness appears.
- After the treatment with 3M HCL, heat the de-ionized water in a beaker is heated for 1-1.5 hours and the treated surface is kept inside it roughly for 15-20 minutes for bringing a uniformity over the surface. The surface now is superhydrophilic in nature.
- To turn it into superhydrophobic, the superhydrophilic surface is taken, kept on a petri dish. After that using a micropipette and setting the volume at 2.5Ml, 4 drops of 1H,1H,2H,2H Perfluorooctylethoxy silane is put around slowly and then allowed into a desiccator for chemical vapour deposition. The air is pumped out from the desiccator, making the interior vacuum for easy CVD to occur. After the CVD process, the surface becomes superhydrophobic in nature.

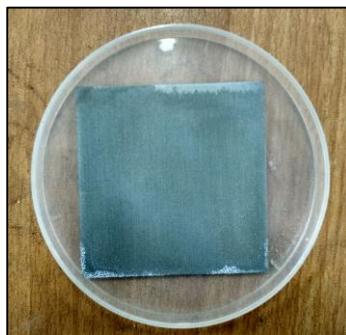


Fig. 2.2i Superhydrophobic surface

2.3 **Synthesis of Nanofluid:**

Low thermal conductivity is a primary limitation in the development of energy efficient heat transfer fluids that are required in various industrial sectors. So, researchers are looking forward for advanced heat transfer fluids which has lower thermo-physical properties like thermal conductivity, viscosity, thermal diffusivity, etc.

In 1873, the technique of enhancing thermal conductivity of fluid by mixing solid particles was proposed, but this failed to achieve the attention of researchers due to different troubles such as erosion, clogging and sedimentation during the flow. [64]

Millimetre and micrometre sized particles can cause clogging of particles, corrosion of components, excess pressure drops, particle sedimentation, etc. So nano sized particles were introduced to solve the problem. Such particles were introduced in a base fluid at a desirable volume fraction. However, the main challenge was to produce homogeneous and stable mixture of nanoparticles and base fluid which was not easy. For stability, surfactants in right proportion need to be used.

Generally, for synthesis two kinds of methods are employed.

- i. Single or One-step method
- ii. Two step method

Here two step method is followed for the synthesis of nanofluids.

2.3.1 **Two-step method of preparation of Nanofluids:**

This method is widely and commonly used for the synthesis of Nanofluids. There are two steps. In the first step, nanoparticles, nanorods, nanofibers, nanotubes, etc., were prepared in dry powder form by hydrothermal synthesis, sol-gel method, microemulsion, etc. The second step involves the dispersion of nanoparticles into the base fluid by magnetic force agitation.

This preparation was done in two step methods. After weighing the nanoparticles with respect to the weight of the base fluid taken as per equation (7) in High accuracy Electric weight balance machine, Cetyltrimethylammonium Bromide (Fig. 2.3.4ii) was added in the ratio 1:10 along with the TiO₂ Nanoparticles which were measured

as per the required volume fraction (0.01vol%, 0.1vol%, 0.5vol%). After measuring amount of surfactant to be used, it was then added into the water and mixed for 2 hours on Magnetic Stirrer (Fig. 2.3.3i) at 600rpm. Magnetic stirring rod of 3cm (Fig. 2.3.3ii) was used for stirring purpose. After stirring was done, the nanoparticles were added and stirred for 2 hours. After mixing, the solution was put on a Bath Sonicator for 2 hours again for homogeneous mixing. The main purpose was to agitate the particles in the solution. It converts the electrical signals into a physical vibration to break substances and disperse them apart. This kind of disruptions can mix solutions.

2.3.2 Measurement of Nanoparticles:

The amount of Nanoparticle to be used during the synthesis was measured using volume fraction equation (7), where ϕ = Volume Fraction of the desired solution,

$$\Phi = \frac{\left(\frac{w}{\rho}\right)_{\text{nanoparticles}}}{\left(\frac{w}{\rho}\right)_{\text{nanoparticles}} + \left(\frac{w}{\rho}\right)_{\text{water}}} \quad (7)$$

Here, w=Weight of the water/nanoparticles.
 ρ =Density of water/nanoparticles. Here three volume fractions were used which are 0.01%, 0.1%, 0.5%. An electronic balance (Fig.2.3.2i) with high accuracy (Sartorius, BSA 224S – CW, max 220g, accuracy 0.1mg) was deployed to weigh the amount of nanoparticles and the surfactant. The electric balance has to be kept on for 45 minutes to stabilize and before using it. The weighing of nanoparticles was done on a butter paper so that the nanoparticles don't stick to the paper before making the solution



Fig. 2.3.2i Electronic Balance

2.3.3 Mixing and Sonication for preparation of Nanofluid:

The mixing of Nanoparticle along with surfactants was done in two step methods. After weighing the nanoparticles in High accuracy Electric weight balance machine (Fig. 2.3.2i), Cetyltrimethylammonium Bromide was added in the ratio 1:10 along with the TiO_2 Nanoparticles. Then calculated amount of water was added in the lab glass bottle in which the nanoparticles and surfactant mixture was put along. After that the mixture was put on a magnetic stirrer (Fig. 2.3.3i) for mixing for 2hours at 600rpm. Magnetic stirrer rod (3cm) was used for stirring. After 2hours of stirring, the solution was put on a Bath sonicator (Fig.) for 2 more hours for homogenous mixing. The main purpose was to agitate the particles in the solution and disrupt the mix solutions. It uses electrical signals to convert it into a physical vibration to break particles apart.



(a)



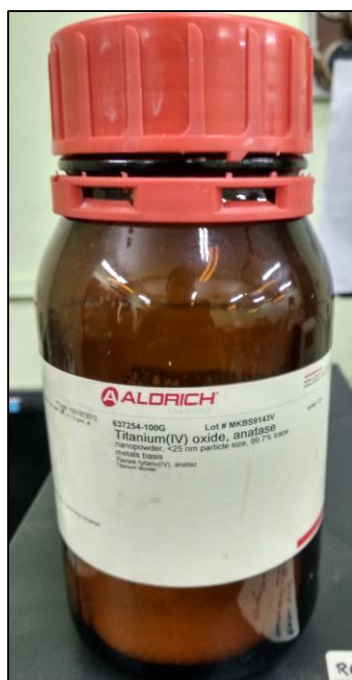
(b)

Fig. 2.3.3 (i) Magnetic stirrer (ii) Magnetic stirring rods

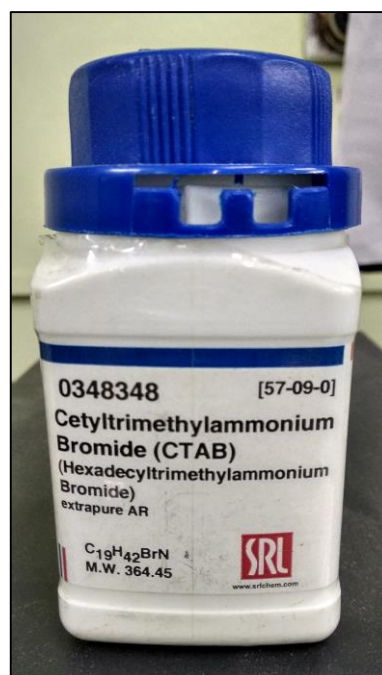
2.3.4 Surfactant:

For preparation of Nanofluids, Cetyltrimethylammonium Bromide (CTAB) was taken in the ratio 1:10=Surfactant: Nanoparticle. It is easy to measure when in the form of powder. For other kind of surfactants like Acetic acid glacial, Oleic Acid

etc. The amount of nanoparticle required was calculated using equation (7) and then required amount of CTAB required was calculated.



(i)



(ii)

Fig. 2.3.4 (i) TiO₂ Nanoparticles (ii) CTAB

After measuring the proper amount of surfactant, it was added into the water and mixed for 2 hours on Magnetic Stirrer. After stirring, the Nanoparticles were added and stirred again for 2 hours. After mixing, the solution was Bath Sonicated for 2 hours again for homogeneous mixing. There was a tendency of precipitation after 1 week of Nanofluid preparation so it is better to perform the experiment within 1 week of Nanofluid preparation for better and accurate results.

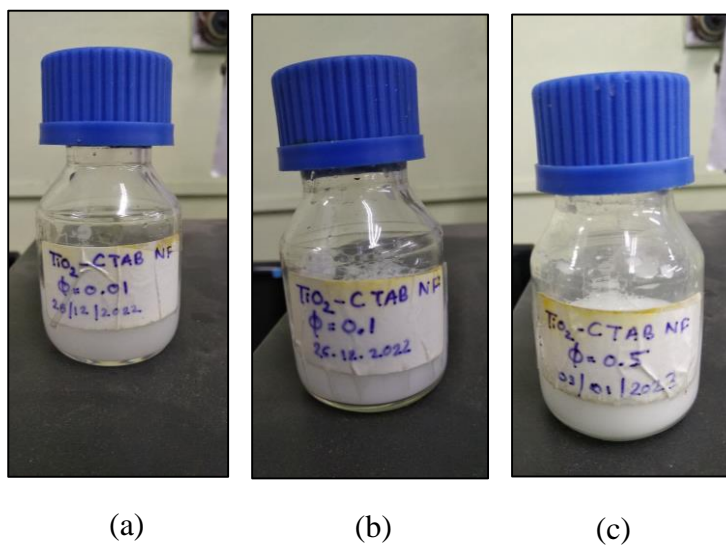


Fig. 2.3.4 TiO₂-CTAB Nanofluids (iii) $\phi=0.01$ (iv) $\phi=0.1$ (v) $\phi=0.5$

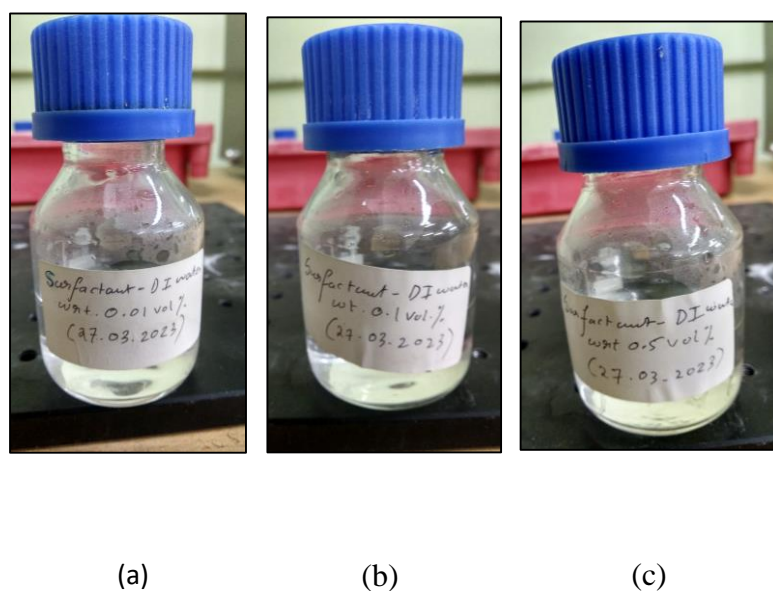


Fig. 2.3.4 CTAB-water solution (vi) 0.12548 mmol/L (vii) 1.14153 mmol/L (viii) 6.19983 mmol/L

2.4 Surface Tension of Nanofluids:

The surface tension of Nanofluids can be measured in various ways. The most common way is the Du Noüy ring experiment. However, there are other methods which involve maximum bubble pressure method where it showed the surface tension of nanofluid was dependent on the temperature and the concentration. An increase of about 5% in the surface tension for a concentration of 1 g/liter nanofluid over the base fluid was reported. [65] Another method involves pendant droplet method which showed experiments on three different volume concentrations. The surface tension decreases with an increase in particle concentration. The surface tension was seen to be a strong function of surfactant concentration. [66] However, the method used in this experiment is Du Noüy ring method.

In this experiment, surface tensiometer (in Fig.2.4a) is used. The Du Noüy ring is attached to the instrument which is used to measure the interfacial surface tension. This is of Platinum material. Before usage, the ring has to be rinsed with acetone at regular intervals and dried for accurate results. It is also better to perform chemical etching to remove the residual particles, rinsed in Acetone, dried for measurement. This method involves pull force action. The radial dial is set to zero point. The ring is dipped into the surface of the solution. Then the dial is rotated. After some time, a meniscus is noticed between the ring and the surface of the water (In Fig.2.4b) After some time, the ring comes out of the solution due to the spring action and the dial indicates the surface tension of the solution at that point. However, there are standard equations by which the surface tension can be measured.

$$P_T = P_R + 4\pi R v_{ideal} \quad (8)$$

$$v = f v_{ideal} \quad (9)$$

where, P_T = Total force on ring

P_R = Weight of the ring

R = Radius of the ring

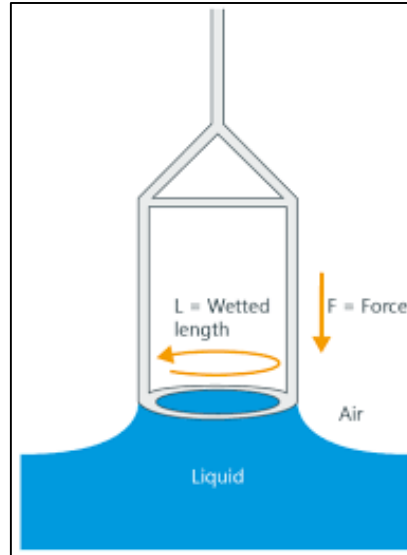
v_{ideal} = Ideal surface tension of the liquid

γ = Surface tension of the liquid

f = Shape factor



(a)



(b)

Fig. 2.4 (i) Surface Tensiometer (ii) Du-Noüy phenomena

2.5 Experimental Setup and Procedure:

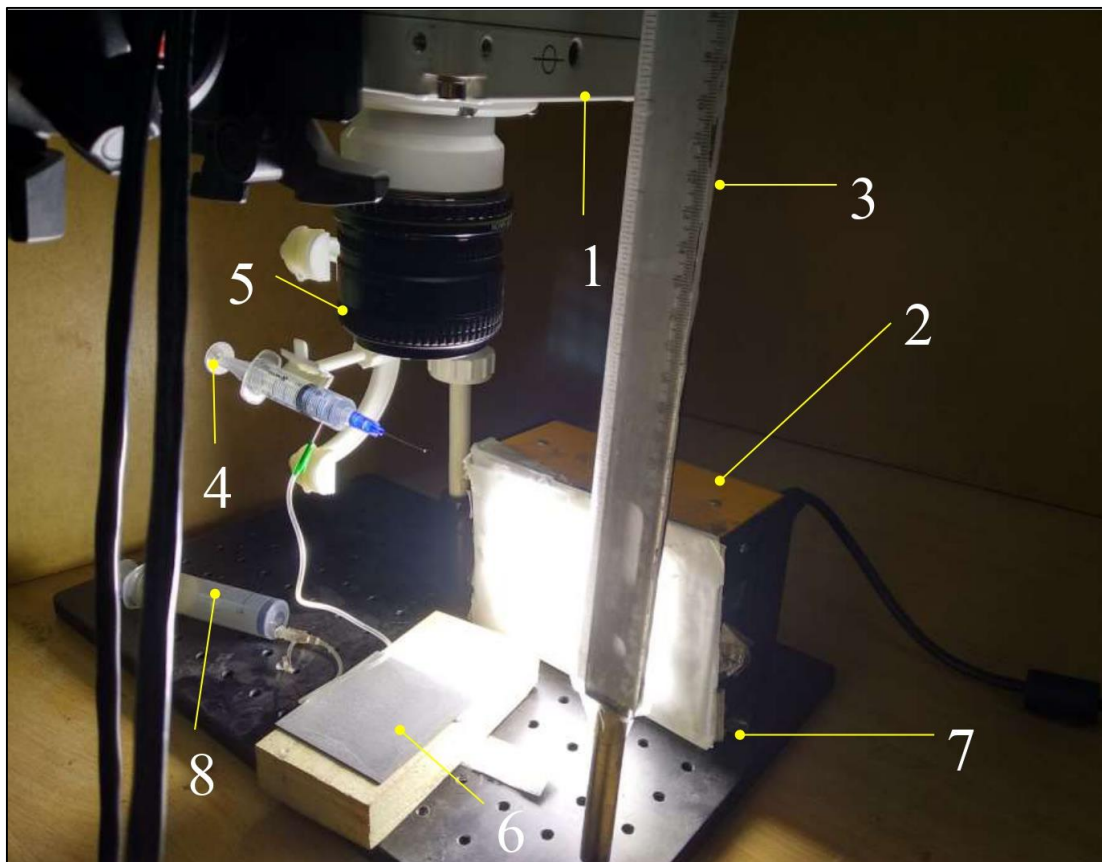


Fig. 2.5i Experimental setup- 1. High Speed camera 2. MultiLED light 3. Scale 4. Syringe with needle 5. Camera lens with extension tube 6. Superhydrophobic surface 7. Optical bench 8. Plunger

An experimental setup was set as shown above. A small optical bench was taken and a hole stand was fixed. Then the retort stand was fixed into the hole stand. The fisher clamp was fixed at certain height. For measuring the height, a scale was fixed over the optical bench rail in vertical position to take note of changing heights. A medical syringe was attached with the fisher clamp with double sided tape. The needles of varied diameter were changed as per the progression of the experiment. The highspeed camera was fixed in a tripod and angled over the needle at 0° . The angle was then measured with clinometer for confirmation and calibrated. The syringe was connected with plunger via butterfly needle for dispensing the droplets over the superhydrophobic surface. As the height was gradually increased, the pancake pattern for the droplets changed. Initially it was performed with water for three different types of needle diameters (0.231 mm, 0.540

mm, 0.714 mm). Then it was done with nanofluids for three different types of volume fractions (0.01%, 0.1%, 0.5%). Before the experiment, the needles were bath sonicated for 10 minutes in acetone.



Fig. 2.5ii Bath sonicator

After that the needle was attached with disposable syringe and fixed with the clamp with the help of double-sided tape. A scale was fixed beside the clamp with the help of optical bench rail to measure the increasing heights from the base. After that the superhydrophobic surface was placed under the clamp at a position where the droplets could be impinged over the superhydrophobic surface. Three kinds of needles were used here. The butterfly needle was attached with the syringe and a plunger was used to dispense the droplets. The drop impinges over the surface and as the drop impinges, the pancake diameter of the drop was established and the entire event was video recorded using high-speed camera at 10,000 fps. To view the entire process through high-speed camera, it was connected with a laptop with PCC application to capture the video/image and a LED lamp was kept beside so that the clear view can be taken. The height of the needle was slowly increased, the drop was impinged and the moment the droplet was impinged and pancake was formed. The entire experiment was performed with an aim to closely analyse the dynamic behaviour of the droplet impingement over superhydrophobic surface. It was done unless the crowning pattern around the perimeter of impinged droplet was noticed and splashing of the droplet occurs.



(a)



(b)



(c)

Fig. 2.5iii Needles used for droplet impingement (a) Blue needle (Diameter: 0.714mm) (b) Yellow needle (Diameter: 0.231mm) (c) Purple needle (Diameter: 0.540mm)

The plunger was used to push the fluid over the surface. It is to note that the volume of each droplet varied according to the needle and also as per the fluid. The plunger was slowly pushed so that the fluid does not come out as jet and falls drop by drop. Each experiment was repeated three times (Base fluid, 0.01%, 0.1%, 0.5%) to verify the experimental uncertainties. While the volumes dispensed were different for different

needles with base fluid, the volumes varied for nanofluid for blue needle (Diameter=0.714mm), yellow needle (Diameter=0.231mm) and purple needle (Diameter=0.540mm). The reason been the surface tension of base fluid differed from that of TiO₂-CTAB nanofluids. The volume was measured by dispensing 20 droplets in a bottle and measuring in precision weighing balance (Fig. 2.3.2i). Then getting the volume of 20 droplets the volume of a single droplet was calculated easily. The bottle was made air tight while measuring to avoid any kind of evaporation. 20 drops were considered to reduce the errors while measuring.



(a)



(b)



(c)

Fig. 2.5iv (a) Vision research AMTEK Phantom high speed camera (b) Nikon AF NIKKOR 50mm 1:1.4D camera lens (c) XIT Extension tube

Table 2.5: Dispensed volume of Droplets for different fluids

➤ **Table 2.5a: Base fluid**

Dispensing needle diameter (mm)	Volume of fluid dispensed (μL)
Blue needle (Diameter=0.714)	13.14
Purple needle (Diameter=0.540)	10.64
Yellow needle (Diameter=0.231)	4.05

➤ **Table 2.5b: 0.01vol% TiO₂-CTAB Nanofluid**

Dispensing needle diameter (mm)	Volume of fluid dispensed (μL)
Blue needle (Diameter=0.714)	9.07
Purple needle (Diameter=0.540)	6.89
Yellow needle (Diameter=0.231)	2.97

➤ **Table 2.5c: 0.1vol% TiO₂-CTAB Nanofluid**

Dispensing needle diameter (mm)	Volume of fluid dispensed (μL)
Blue needle (Diameter=0.714)	8.57
Purple needle (Diameter=0.540)	5.88
Yellow needle (Diameter=0.231)	2.61

➤ **Table 2.5d: 0.5vol% TiO₂-CTAB Nanofluid**

Dispensing needle diameter (mm)	Volume of fluid dispensed (μL)
Blue needle (Diameter=0.714)	7.36
Purple needle (Diameter=0.540)	6.18
Yellow needle (Diameter=0.231)	2.66

After the videos were captured with the help of PCC 3.6 software and high speed camera, images were extracted in tif format to measure the maximum diameter of impinged droplet with the help of ImageJ software. The measurements were done at various angles of 0°, 60° and 120° to reduce the errors during measurements.

Chapter-3

3. Results and discussion

3.1 Surface Tension of Nanofluids

3.1.1 Surface Tension variation with concentration of Nanofluids

For preparation of Nanofluids, first a measured quantity (which depends on the target concentration of the nanofluid) of surfactant was mixed with the base fluid (Water) and then the requisite mass of nanoparticles was mixed and ultrasonicated. Surface tension of the nanofluid was measured with the help of surface tensiometer using du-Nouy ring method. As reference value, the surface tension of the surfacted water was also measured using the same tensiometer. A decreasing trend was observed for surfacted fluid with respect to surfactant concentration whereas for nanofluids the surface tension was found to increase with particle concentration (see Table 3.1)

Table 3.1: Surface Tension of Nanofluids and Surfacted Base Fluid

Concentration of Nanofluids (vol%)	Concentration of Surfactants (mmol/L)	Surface Tension of Nanofluids (mN/m)	Surface Tension of Surfacted Base Fluid (mN/m)
0.01	0.12548	32.02	39.38
0.1	1.14153	35.09	39.14
0.5	6.19983	35.22	36.32

3.2 Impingement dynamics of Nanofluid droplets over Superhydrophobic surface

Figure 3.2i shows the impact behavior of 0.5vol% of nanofluid droplet of diameter 0.24cm and Weber number of 131.62 over the superhydrophobic surface. The figure shows different stages of the droplet impact. Fig. 3.2i (a) shows the droplet at 0 ms, that is, the time of its dispensing from the needle. The droplet remains spherical until the moment it touches the surface (see Fig. 3.2i(b)). Post impact, it spreads radially in the shape of a pancake, spreading to the largest radius, and then recedes. Figure 3.2i (c) shows the droplet on attaining the maximum diameter, while the frame (d) shows the moments after the droplet had started receding. Receding continues till the liquid front reaches a minimum value (see Fig. 3.2i(e)), generating an elongated droplet (not visible in the top view).

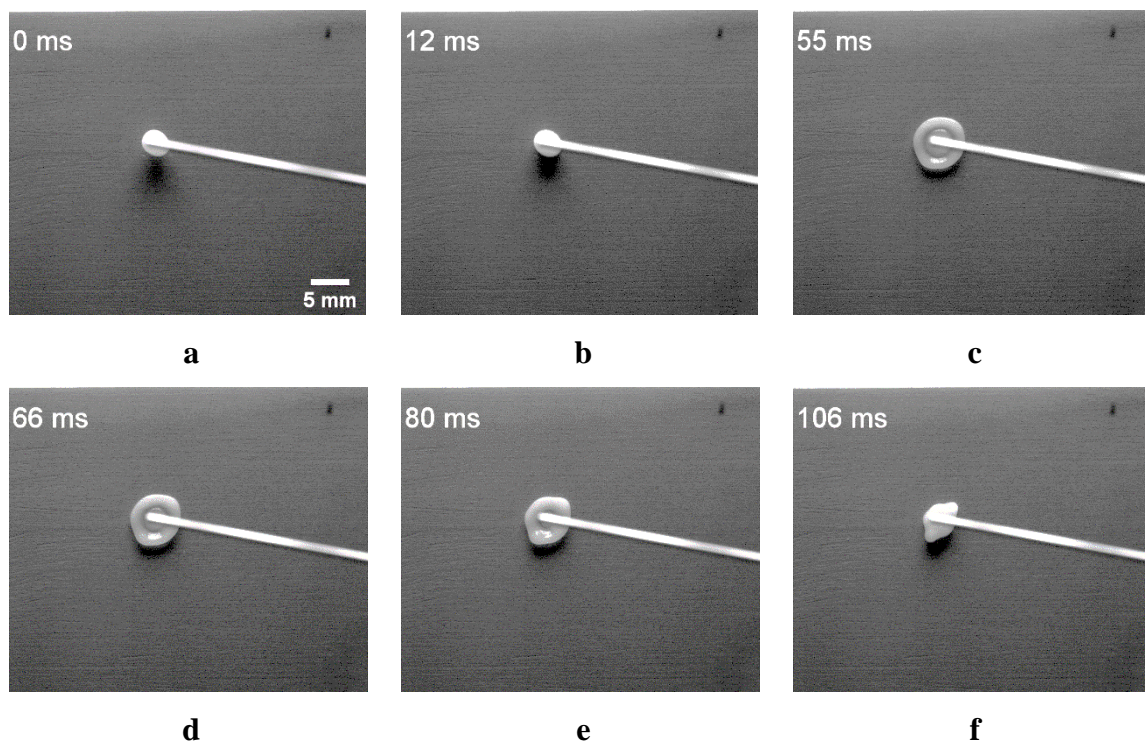


Fig. 3.2i Impact dynamics of a 0.24cm diameter nanofluid droplet (0.5 vol%, Weber Number 131.62) (a)-(f) shows different stages of dynamics over superhydrophobic surface.

However, the momentum of the receding front, and the associated kinetic energy keeps the droplet sloshing (see the bulging of the liquid front in Fig 3.2i(f)) back and forth, until the

kinetic energy dissipates through viscous damping. At this low value of We , the droplet remains attached to the surface throughout the entire period of impact.

Impact behavior changes for droplet with higher impact velocity (droplet released from a greater height). Figure 3.2ii shows the impact behavior of 0.5vol% of nanofluid droplet of diameter 0.24cm and Weber number of 427.75 over superhydrophobic surface. The figure shows different stages of the droplet impact. Frame (a) shows the droplet at 0ms, that is, the time of its dispensing from the needle. Frame (b) shows the moments after the droplet had touched the surface. Frame (c) shows the droplet after attaining the maximum diameter while the crowns are discernable along its perimeter. In this case the droplet splashes and satellite droplets are formed. Frame (d) shows the moments after the droplet had started receding. While receding, large fingerlike structures are formed along the droplet perimeter as the liquid front keeps receding. Here, some of the satellite droplets remain along the extensions as Frame (e) shows the moments before the droplet completely recedes. Frame (f) shows the receding droplet on the superhydrophobic surface.

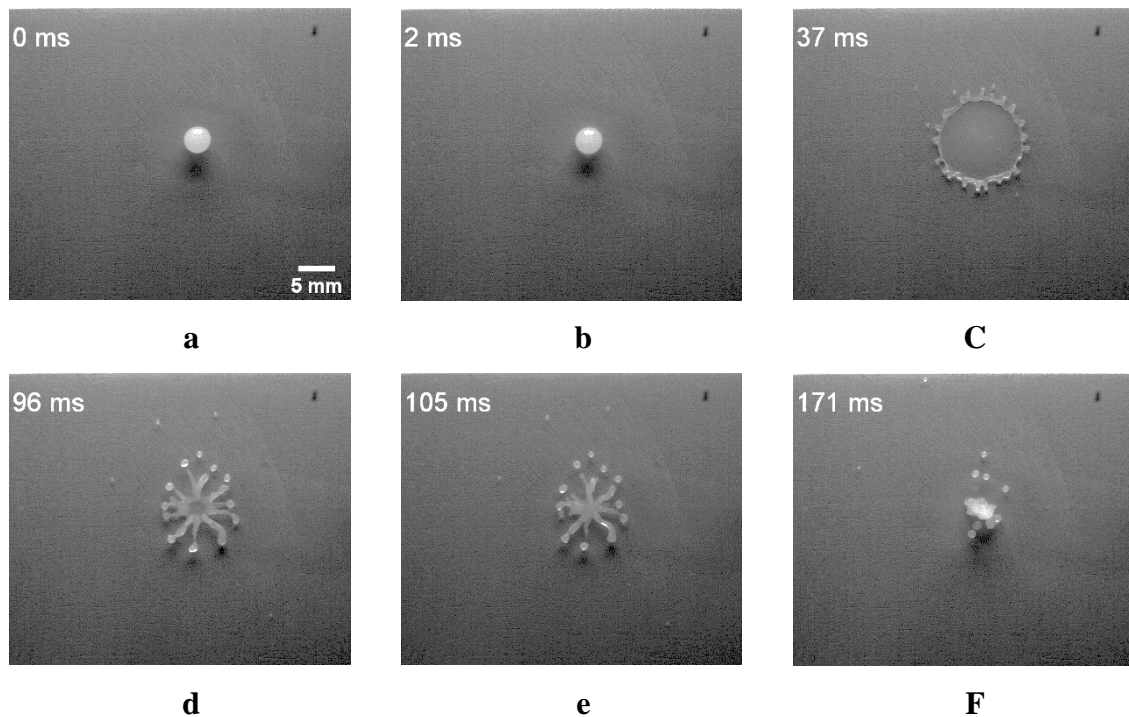


Fig. 3.2ii Impact dynamics of a 0.24mm diameter nanofluid droplet (0.5 vol%, Weber Number 427.75) (a)-(f) shows different stages of dynamics over superhydrophobic surface.

Fig 3.2iii shows the impact behavior of 0.5vol% of nanofluid droplet of diameter 0.24cm and Weber number of 493.56 over superhydrophobic surface from a different perspective, so as

to bring out the features that were missing from the front view. The figure shows different stages of the droplet impact. Frame (a) shows the droplet at 0ms, that is, the time of its dispensing from the needle. Frame (b) shows the moment when the droplet had just touched the surface. Frame (c) shows the pancake-shaped impinged droplet after attaining the maximum diameter while the crowns are being observed along its perimeter. Frame (d) shows the moments after the impinged droplet had started receding. During receding, this view also shows the presence of large fingerlike extensions along the droplet perimeter as the diameter reduces. The satellite droplets are also seen to be formed. Frame (e) shows the moments before the droplet completely recedes. The extensions become more fine and thicker. Frame (f) clearly shows the formation of the oblong shape droplet as the receding front of the liquid pancake collides at the center and forms a Worthington jet [67].

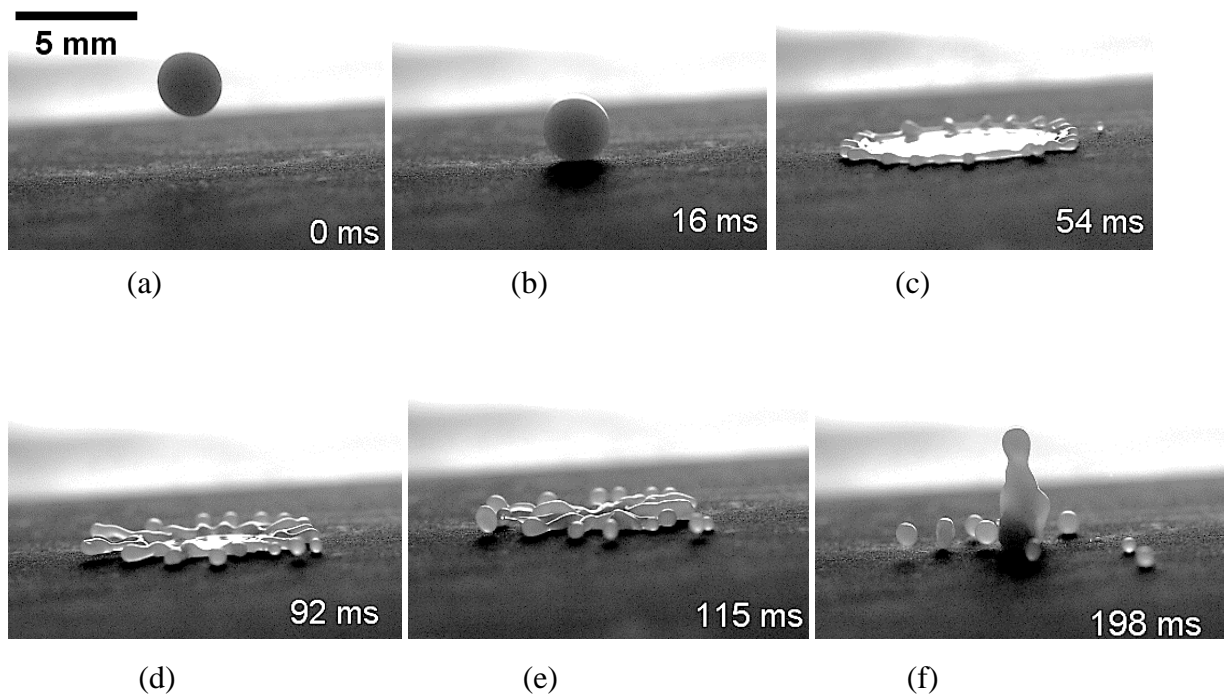


Fig. 3.2iii Impact dynamics of a 0.24mm diameter nanofluid droplet (0.5 vol%, Weber Number 493.56) (a)-(f) shows different stages of dynamics over superhydrophobic surface.

3.2.1 Effect of droplet diameter, impact Weber number and Parametric variation:

To ascertain the role of impacting droplet diameter, impact velocity and nanoparticle concentration on the droplet impact dynamics, parametric study has been conducted under droplets of different diameters (by using three different dispensing needles having diameters of 0.714, 0.540 and 0.231mm), different impact Weber number (by using different impact height) and using Anatase nanofluids under different particle concentrations. For easy benchmarking, a base case with only the base fluids (i.e., deionized water without nanoparticles) has also been studied. Table 3.3a shows different data for base fluid droplet impingement. Needles of internal diameter were used for dispensing the droplet on superhydrophobic surface and the dynamic behavior was carefully analysed with respect to Weber number and Spread factor.

Table 3.3a: Droplet impinging data for the base fluid:

Needle (internal diameter)	Height of impingement (in cm)	Velocity (in cm/s)	Maximum spread diameter(in cm)	Weber number	Spread factor
Blue (0.714mm)	3	76.68	0.94	23.91	3.19
	4	88.54	0.79	31.88	2.72
	5	98.99	0.82	39.85	2.91
	6	108.44	0.90	47.83	3.10
	7	117.13	0.95	55.80	3.30
	8	125.21	1.04	63.77	3.55
	8.5	129.07	1.05	67.76	3.62
	9	132.81	1.12	71.74	3.85
	10	140	1.087	79.71	3.69
	11	146.83	1.138	87.69	3.78
	12	153.36	1.24	95.66	4.34
	13	159.62	1.23	103.63	4.14
	14	165.65	1.335	111.60	4.69
Purple (0.540mm)	3	76.68	0.64	22.29	2.28
	4	88.54	0.68	29.72	2.58
	5	98.99	0.59	37.15	2.02
	6	108.44	0.59	44.59	2.27
	7	117.13	0.663	52.02	2.42
	8	125.21	0.742	59.45	2.68
	9	132.81	0.8	66.88	2.85

	9.5	136.45	0.79	70.60	2.92
	10	140	0.86	74.31	3.19
	11	146.83	0.83	81.74	2.94
	11.5	150.13	0.89	85.46	3.28
	12	153.36	0.91	89.18	3.31
	13	159.62	0.97	96.61	3.63
	14	165.65	0.94	104.04	3.43
	15	171.46	1.07	111.47	4.07
Needle (internal diameter)	Height of impingement (in cm)	Velocity (in cm/s)	Maximum spread diameter(in cm)	Weber number	Spread factor
Yellow (0.231mm)	3.5	82.82	0.62	18.85	3.17
	4.5	93.91	0.702	24.24	3.48
	5.5	103.82	0.702	29.63	3.80
	6.5	112.87	0.54	35.024	2.83
	7.5	121.24	0.603	40.41	2.96
	8.5	129.07	0.63	45.80	3.17
	9.5	136.45	0.689	51.18	3.45
	10.5	143.45	0.66	56.57	3.55
	11	146.83	0.71	59.27	3.69
	11.5	150.13	0.71	61.96	3.69
	12	153.36	0.77	64.65	4.06
	13	159.62	0.76	70.04	3.84
	14	165.65	0.83	75.43	4.17
	15	171.46	0.83	80.82	4.16

Table 3.3b shows different data for 0.01vol% Nanofluid droplet impingement. Needles of internal diameter 0.714mm, 0.540mm and 0.231mm were used for dispensing the droplet on superhydrophobic surface and the dynamic behavior was carefully analysed with respect to Weber number and Spread factor.

Table 3.3b: Droplet impinging data due to 0.01vol% Nanofluid:

Needle (internal diameter)	Height of impingement (in cm)	Velocity (in cm/s)	Maximum spread diameter(in cm)	Weber number	Spread factor
Blue (0.714mm)	2.5	70	0.60	40.74	2.34
	3.5	82.82	0.74	57.04	2.89
	4.5	93.91	0.74	73.34	2.88
	5.5	103.82	0.56	89.63	2.19

Needle (internal diameter)	Height of impingement (in cm)	Velocity (in cm/s)	Maximum spread diameter(in cm)	Weber number	Spread factor
	6.5	112.87	0.71	105.93	2.77
	7.5	121.24	0.71	122.23	2.76
	8.5	129.07	0.72	138.53	2.80
	9.5	136.45	0.85	154.83	3.31
	10.5	143.45	0.77	171.12	3.00
	11.5	150.13	0.89	187.42	3.45
	12	153.36	0.87	195.57	3.39
	12.5	156.52	1.01	203.72	3.93
Purple (0.540mm)	2.5	70	0.58	37.18	2.48
	3.5	82.82	0.66	52.05	2.82
	4.5	93.91	0.61	66.93	2.60
	5.5	103.82	0.49	81.80	2.07
	6.5	112.87	0.49	96.68	2.08
	7.5	121.24	0.49	111.55	2.08
	8.5	129.07	0.65	126.42	2.76
	9.5	136.45	0.64	141.30	2.72
	10.5	143.45	0.68	156.17	2.88
	11.5	150.13	0.72	171.05	3.05
	12	153.36	0.63	178.48	2.68
	12.5	156.52	0.69	185.92	2.94
Yellow (0.231mm)	2.5	70	0.48	28.10	2.74
	3.5	82.82	0.53	39.34	3.00
	4.5	93.91	0.61	50.58	3.44
	5.5	103.82	0.39	61.82	2.22
	6.5	112.87	0.41	73.06	2.29
	7.5	121.24	0.46	84.30	2.57
	8.5	129.07	0.46	95.54	2.58
	9.5	136.45	0.52	106.78	2.91
	10.5	143.45	0.51	118.02	2.84
	11.5	150.13	0.56	129.26	3.15
	12	153.36	0.57	134.88	3.21
	12.5	156.52	0.607	140.50	3.40

Table 3.3c shows different data for 0.01vol% Nanofluid droplet impingement. Needles of internal diameters 0.714mm, 0.540mm and 0.231mm were used for dispensing the droplet on

superhydrophobic surface and the dynamic behavior was carefully analysed with respect to Weber number and Spread factor.

Table 3.3c: Droplet impinging data due to 0.1vol% Nanofluid:

Needle (internal diameter)	Height of impingement (in cm)	Velocity (in cm/s)	Maximum spread diameter(in cm)	Weber number	Spread factor
Blue (0.714mm)	3	76.68	0.63	54.88	2.49
	4	88.54	0.71	73.18	2.81
	5	98.99	0.56	91.48	2.20
	6	108.44	0.60	109.77	2.37
	7	117.13	0.69	128.07	2.74
	8	125.21	0.66	146.36	2.60
	9	132.81	0.75	164.66	2.96
	9.5	136.45	0.76	173.81	3.00
	10	140	0.78	182.96	3.09
	11	146.83	0.80	201.25	3.18
	11.5	150.13	0.86	210.40	3.41
	12.5	156.52	0.88	228.70	3.49
	13	159.62	0.89	237.85	3.53
	13.5	162.66	0.95	246.99	3.72
	14	165.65	0.92	256.14	3.61
Purple (0.540mm)	3	76.68	0.50	48.40	2.25
	4	88.54	0.59	64.53	2.63
	5	98.99	0.67	80.66	2.98
	6	108.44	0.46	96.80	2.08
	7	117.13	0.53	112.93	2.38
	8	125.21	0.57	129.06	2.57
	9	132.81	0.59	145.20	2.67
	10	140	0.63	161.33	2.82
	11	146.83	0.67	177.46	2.98
	12	153.36	0.74	193.60	3.28
	13	159.62	0.76	209.73	3.38
	13.5	162.66	0.82	217.80	3.66
	14	165.65	0.84	225.86	3.72
Yellow (0.231mm)	3	76.68	0.48	36.94	2.81
	4	88.54	0.52	49.25	3.08

Needle (internal diameter)	Height of impingement (in cm)	Velocity (in cm/s)	Maximum spread diameter(in cm)	Weber number	Spread factor
	5	98.99	0.36	61.57	2.11
	6	108.44	0.47	73.88	2.75
	7	117.13	0.42	86.19	2.47
	8	125.21	0.46	98.50	2.73
	9	132.81	0.48	110.82	2.86
	10	140	0.52	123.13	3.04
	11	146.83	0.56	135.45	3.27
	12	153.36	0.54	147.76	3.17
	13	159.62	0.58	160.07	3.39
	13.5	162.66	0.58	166.23	3.39
	14	165.65	0.63	172.39	3.67

Table 3.3b shows different data for 0.01vol% Nanofluid droplet impingement. Needles of internal diameters 0.714mm, 0.540mm and 0.231mm were used for dispensing the droplet on superhydrophobic surface and the dynamic behavior was carefully analysed with respect to Weber number and Spread factor.

Table 3.3d: Droplet impinging data due to 0.5vol% Nanofluid:

Needle (internal diameter)	Height of impingement (in cm)	Velocity (in cm/s)	Maximum spread diameter(in cm)	Weber number	Spread factor
Blue (0.714mm)	3	76.68	0.66	98.71	2.73
	4	88.54	0.63	131.61	2.63
	5	98.99	0.67	164.52	2.79
	6	108.44	0.75	197.42	3.13
	7	117.13	0.80	230.32	3.34
	8	125.21	0.83	263.23	3.46
	9	132.81	0.85	296.13	3.54
	10	140	0.94	329.04	3.90
	11	146.83	0.95	361.94	3.94
	11.5	150.13	0.97	378.39	4.00
	12	153.36	0.99	394.85	4.10
	13	159.62	1.07	427.75	4.43
Purple (0.540mm)	3	76.68	0.64	93.14	2.83
	4	88.54	0.50	124.18	2.23

Needle (internal diameter)	Height of impingement (in cm)	Velocity (in cm/s)	Maximum spread diameter(in cm)	Weber number	Spread factor
	5	98.99	0.57	155.23	2.53
	6	108.44	0.65	186.28	2.89
	7	117.13	0.71	217.33	3.13
	8	125.21	0.73	248.37	3.23
	9	132.81	0.75	279.42	3.32
	10	140	0.79	310.47	3.49
	11	146.83	0.82	341.51	3.60
	12	153.36	0.81	372.56	3.58
	12.5	156.52	0.93	388.09	4.09
	13	159.62	0.86	403.61	3.81
	14	165.65	0.93	434.66	4.12
	15	171.46	0.93	465.70	4.10
Yellow (0.231mm)	3	76.68	0.52	70.35	3.04
	4	88.54	0.59	93.80	3.47
	5	98.99	0.44	117.25	2.58
	6	108.44	0.48	140.70	2.80
	7	117.13	0.53	164.16	3.13
	8	125.21	0.57	187.61	3.32
	9	132.81	0.60	211.06	3.53
	10	140	0.61	234.51	3.58
	11	146.83	0.66	257.96	3.87
	12	153.36	0.70	281.41	4.09
	13	159.62	0.72	304.87	4.19
	14	165.65	0.74	328.32	4.30
	14.5	168.58	0.75	340.04	4.38
	15	171.46	0.78	351.77	4.54

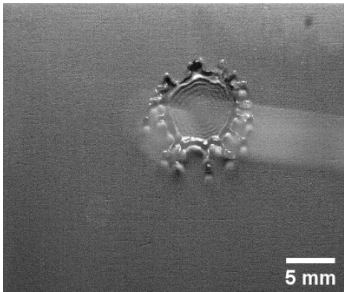
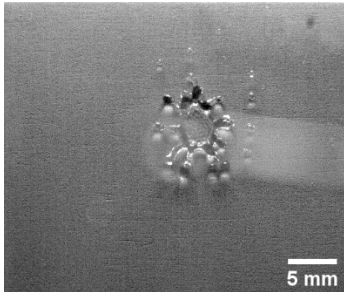
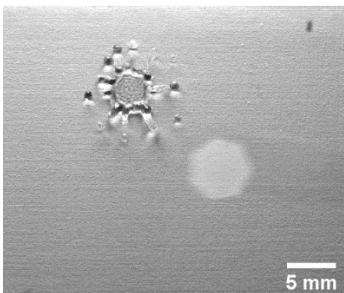
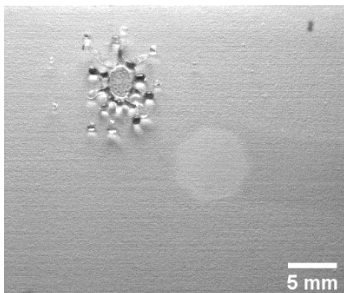
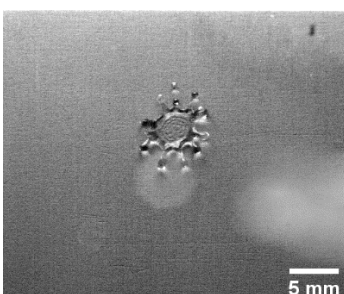
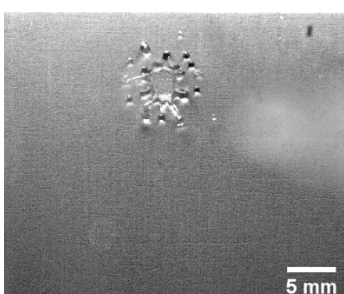
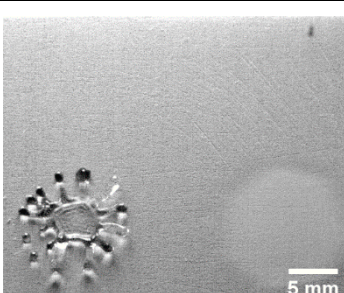
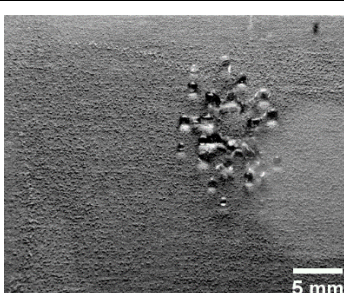
3.2.2 Impingement characteristics:

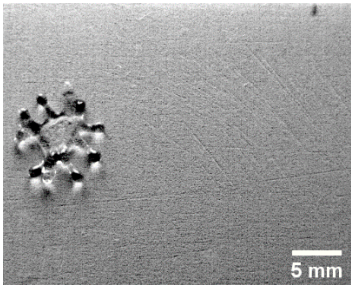
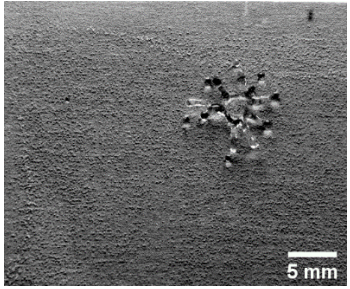
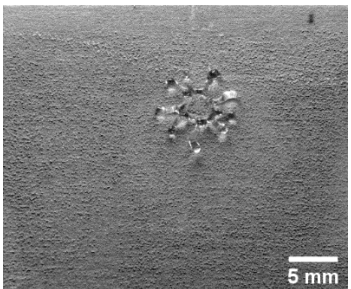
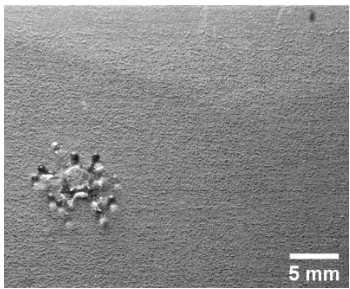
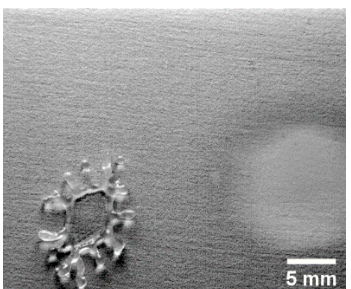
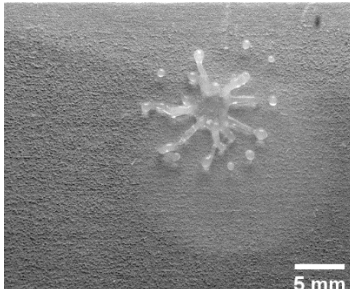
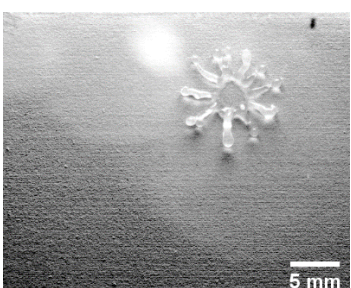
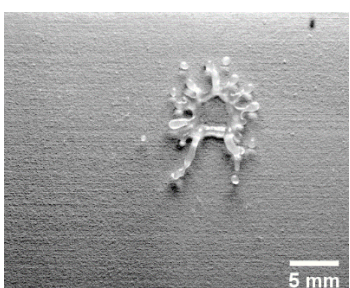
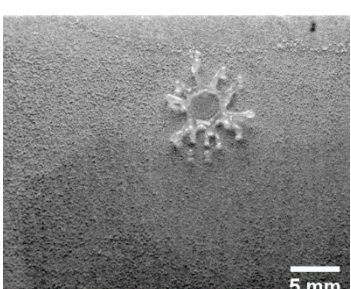
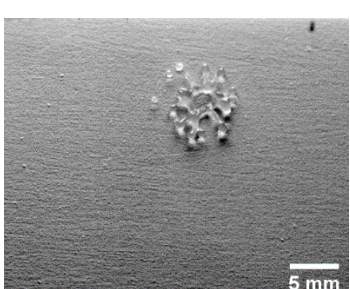
3.2.2a Impingement characteristics for base fluid:

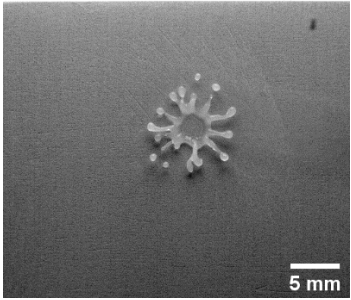
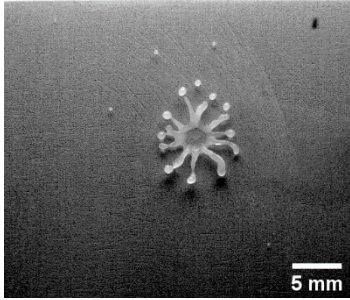
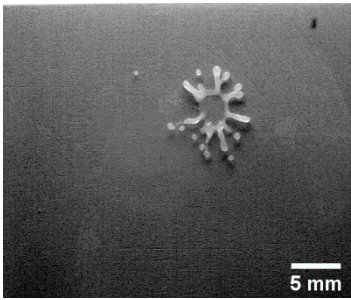
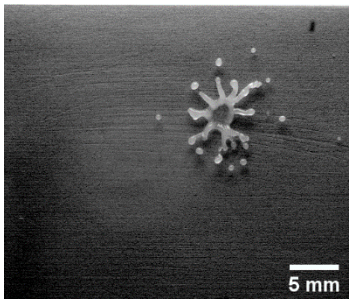
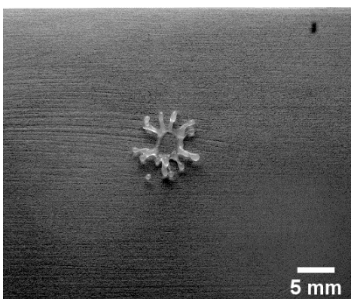
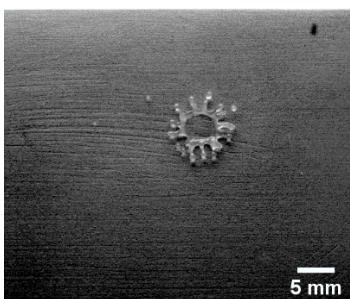
Table 3e represents the crowning and splashing behavior for various concentration of fluids over Superhydrophobic surface. For particle concentration of 0 vol% which is for the base fluid (water), the critical Weber number for which the crowning occurs is 63.77 and the critical Weber number for which the splashing occurs is 67.76 for the droplet diameter of 0.29cm

(Internal needle diameter=0.714mm). Similarly, droplet diameter of 0.19cm (Internal needle diameter=0.231mm) shows the critical Weber number for crowning as 61.96 and critical Weber number for splashing as 64.65. It is observed that for smaller droplet diameter, the critical crowning Weber number and critical splashing Weber number is smaller as compared to the larger dispensing needles.

Table 3.3e: Crowning and splashing events for different concentration of fluids:

Particle conc	Needle (in mm)	Droplet dia (in cm)	We_{crown}	Event	We_{splash}	Event
0	0.714	0.29	63.77		67.76	
	0.540	0.27	85.46		89.18	
	0.231	0.19	61.96		64.65	
0.01	0.714	0.25	187.42		195.57	

Particle conc	Needle (in mm)	Droplet dia (in cm)	We_{crown}	Event	We_{splash}	Event
	0.540	0.23	171.05		178.48	
	0.231	0.17	134.88		140.50	
0.1	0.714	0.25	228.70		237.85	
	0.540	0.22	217.80		225.86	
	0.231	0.17	166.23		172.39	

Particle conc	Needle (in mm)	Droplet dia (in cm)	We_{crown}	Event	We_{splash}	Event
0.5	0.714	0.24	378.39		394.85	
	0.540	0.22	372.56		388.09	
	0.231	0.17	328.32		340.04	

3.2.2b Impingement characteristics for 0.01vol % Nanofluid:

Table 3e describes the crowning and splashing behavior for 0.01vol% TiO₂ Nanofluid. Because of low particle concentration, the behavior was no different from the base fluid. However, due to the indifferences in the surface tension, the Weber number varied. The critical Weber number for which the crowning occurs is 187.42 and the critical Weber number for which the splashing occurs is 195.57 for the droplet diameter of 0.26 cm (dispensed from the 0.714mm diameter needle). Similarly, droplet diameter of 0.17cm (Internal needle diameter=0.231mm) shows the critical Weber number for crowning as 134.88 and critical Weber number for splashing as 140.50.

3.2.2c Impingement characteristics for 0.1vol % Nanofluid:

Table 3e contains the crowning and splashing behavior for 0.1vol% TiO₂ Nanofluid. In this case, the particle concentration is relatively larger than the previous case. However, due to the indifferences in the surface tension, the Weber number varies for different droplet diameters. The critical Weber number for which the crowning occurs is 228.70 and the critical Weber number for which the splashing occurs is 237.85 for the droplet diameter of 0.25cm (Internal needle diameter=0.714mm). For a slightly smaller droplet diameter (0.22cm; Internal diameter=0.540mm), the critical Weber number for crowning and critical Weber number for splashing were 217.80 and 225.86 respectively. Similarly, droplet diameter of 0.17cm (Internal needle diameter=0.231mm) shows the critical Weber number for crowning as 166.23 and critical Weber number for splashing as 172.39. However, while investigating the spreading and receding behavior, the crown formed along the droplet perimeter were larger in sizes.

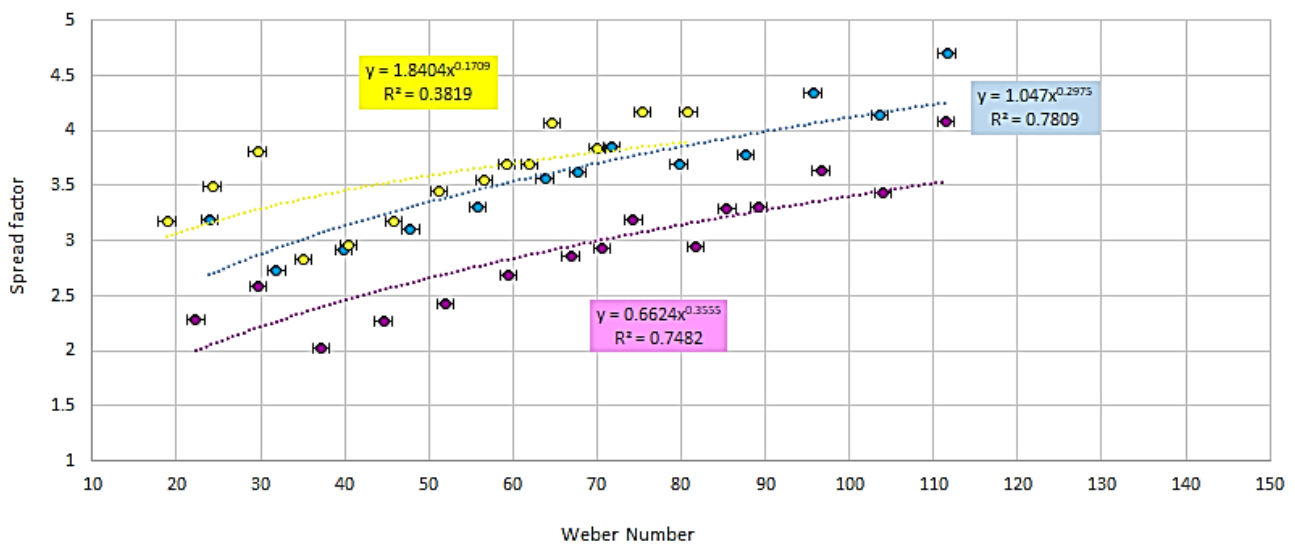
3.2.2d Impingement characteristics for 0.5vol % Nanofluid:

The table 3e contains the crowning and splashing behavior for 0.5vol% TiO₂ Nanofluid. In this case, the particle concentration is significantly higher than the previous three cases. However, due to the indifferences in the surface tension, the Weber number varies for different droplet diameters. The critical Weber number for which the crowning occurs is 378.39 and the critical Weber number for which the splashing occurs is 394.39 for the droplet diameter of 0.24cm (Internal needle diameter=0.714mm). Similarly, droplet diameter of 0.17cm (Internal needle diameter=0.231mm) shows the critical Weber number for crowning as 328.32 and critical Weber number for splashing as 340.34. However, while investigating the spreading and receding behavior, the crown formation along the perimeter of the impinged droplet were larger in sizes and more prominent than the previous three cases.

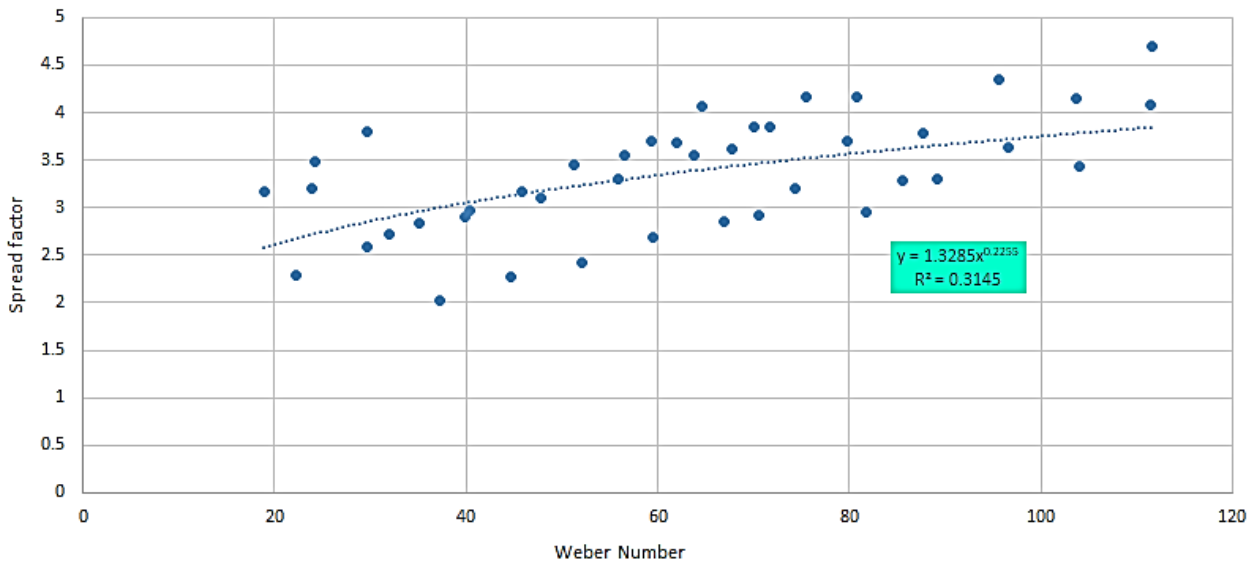
3.2.3 Spread factor vs Weber number characteristic curves:

3.2.3a Spread factor vs Weber number characteristic curve for base fluid:

For dispensing the base fluid, three needles were used that had diameters of 0.714mm, 0.540mm and 0.231mm. The variation of spread factor with Weber number is shown in Fig. 3.2.3i. For all the three dispensing needles, the curves are found to follow power law. The data points in the plot are aligned with the data furnished in Table 3.3a. Base fluid droplets dispensed from the needle with minimum diameter show a non-monotonic behavior with a discontinuity around $We = 29.63$. A close observation of the impacted droplet image (Table 3.3e and Table 3.3a) indicates a transition from smooth pancake shape to a disk surrounded with annular crown. For the other two cases (droplets dispensed from larger needles) such shift is not observed.



(a)

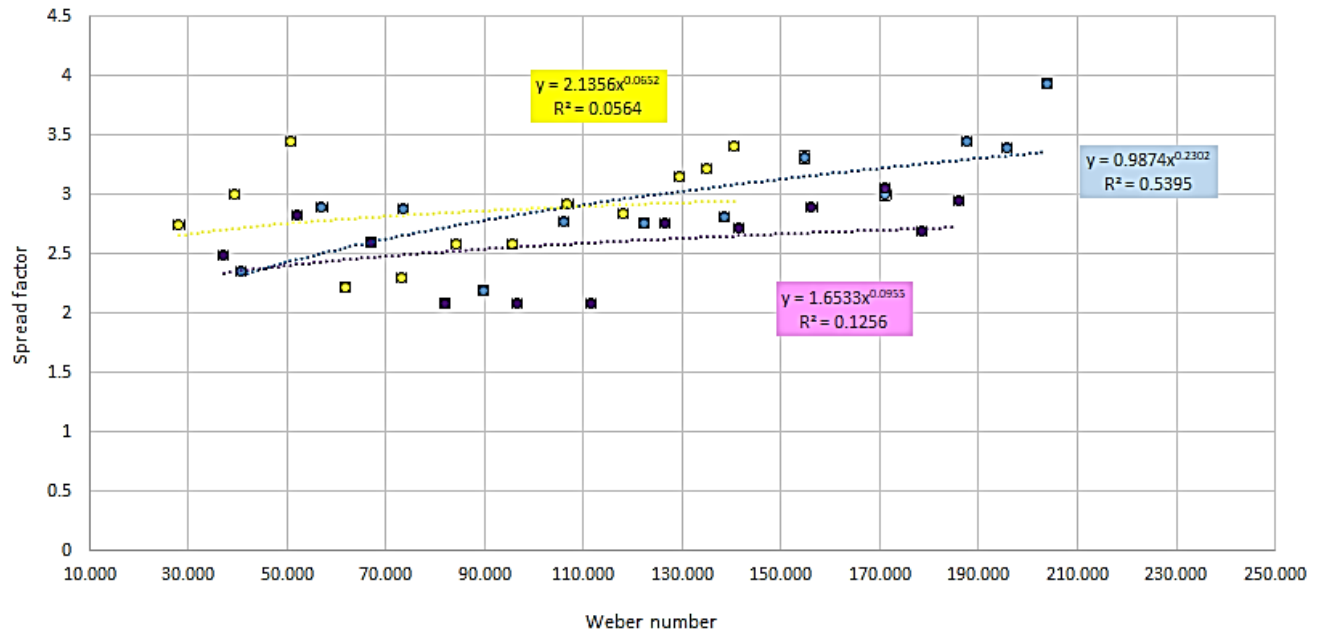


(b)

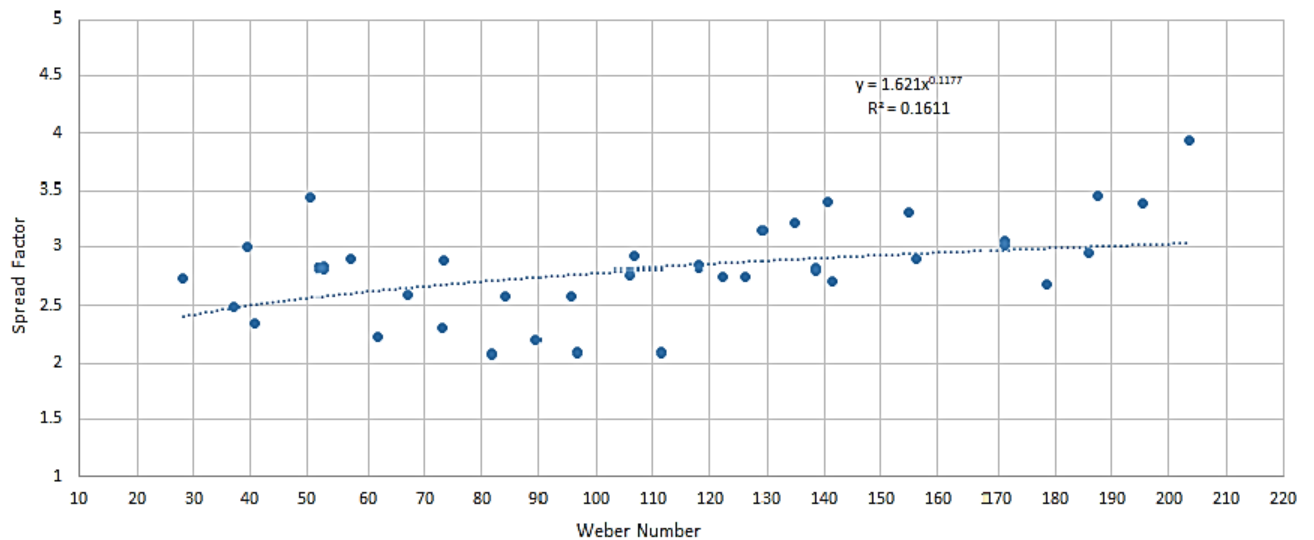
**Fig. 3.2.3i (a) Spread factor vs Weber number for all kinds of needles used for base fluid
(b) Spread factor vs Weber number for all needles combined used for base fluid**

3.2.3b Spread factor vs Weber number characteristic curve for 0.01 vol% nanofluid:

For dispensing the nanofluid droplet of 0.01vol%, three needles were used that had diameters of 0.714mm, 0.540mm and 0.231mm. The variation of spread factor with Weber number is shown in Fig. 3.2.3ii. For all the three dispensing needles, the curves are found to follow power law. The data points in the plot are aligned with the data furnished in Table 3.3b. Nanofluid droplets dispensed from the needle with minimum diameter show a non-monotonic behavior with a discontinuity around $We = 50.58$. A close observation of the impacted droplet image (Fig 3.3b and Table 3.3e) indicates a transition from smooth pancake shape to a disk surrounded with annular crown. For the other two cases (droplets dispensed from larger needles) such shift is not observed.



(a)



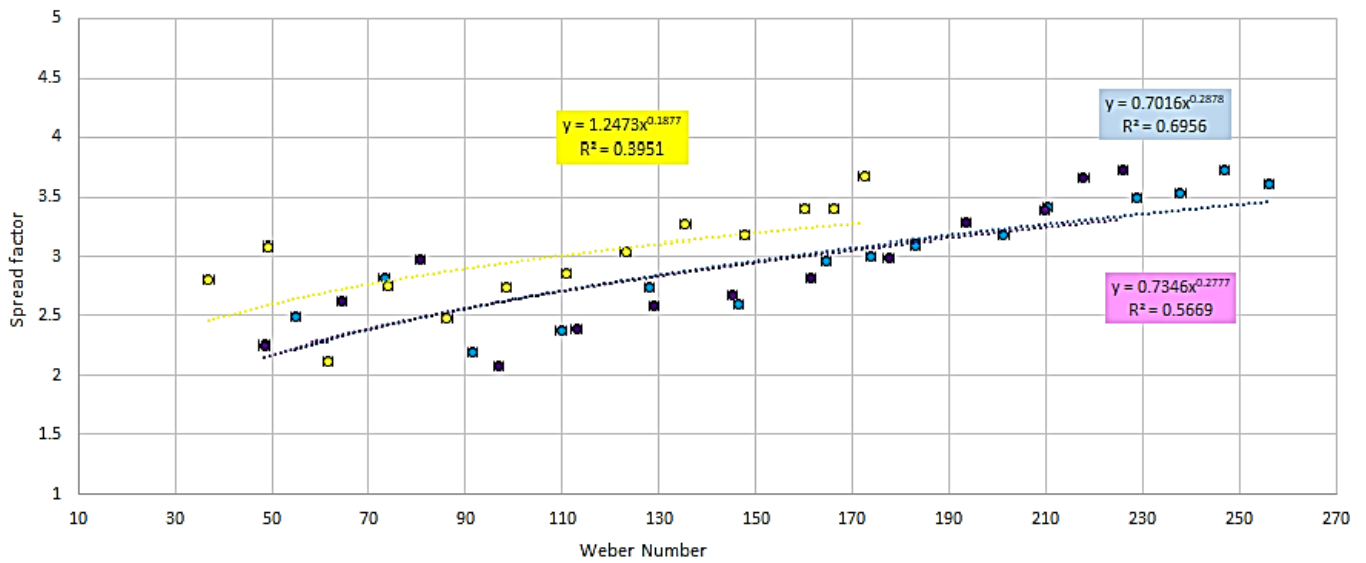
(b)

Fig. 3.2.3ii (a) Spread factor vs Weber number for all kinds of needles used for 0.01 vol% nanofluid
(b) Spread factor vs Weber number for all needles combined used for 0.01 vol% nanofluid

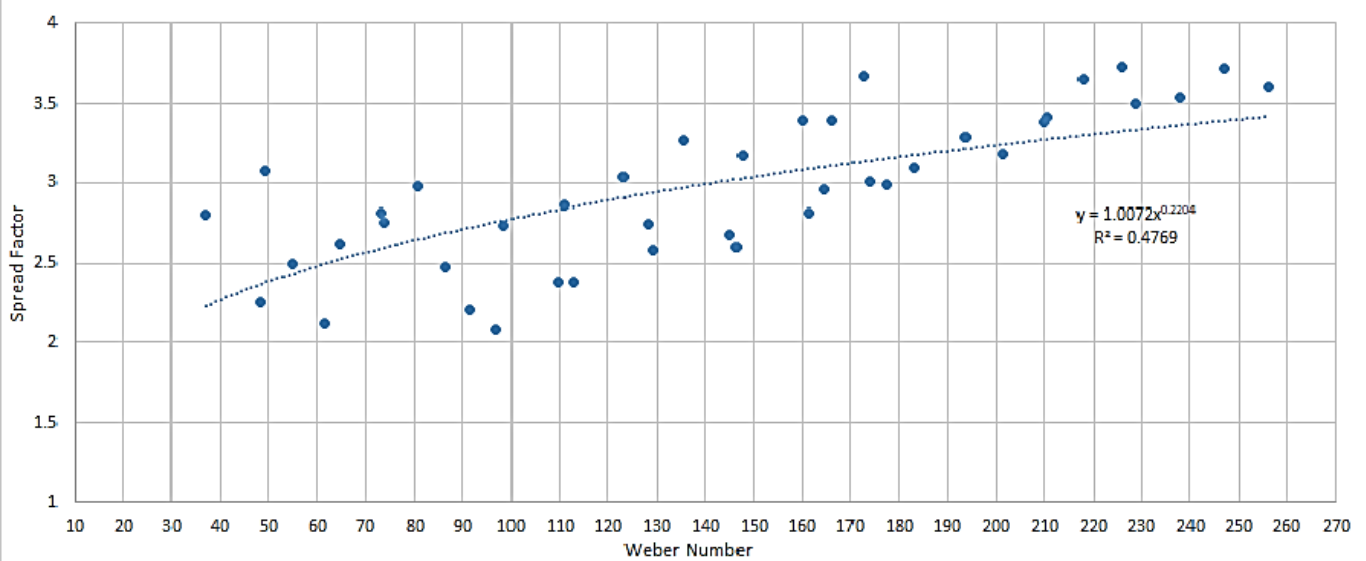
3.2.3c Spread factor vs Weber number characteristic curve for 0.1 vol% nanofluid:

For dispensing the base fluid, three needles were used that had diameters of 0.714mm, 0.540mm and 0.231mm. The variation of spread factor with Weber number is shown

in Fig. 3.2.3iii. For all the three dispensing needles, the curves are found to follow power law relationship. The data points in the plot are aligned with the data furnished in Table 3.3c. Nanofluid droplets dispensed from the needle with minimum diameter show a non-monotonic behavior with a discontinuity around $We = 49.25$. A non-monotonic behavior was also observed around $We=80.67$ for the droplet dispensed from the 0.540mm diameter needle. However, for needles with diameters 0.540mm and 0.231mm, the trendline merged together indicating match in data points as per Table 3.3c. A close observation of the impacted droplet image (Table 3.3e) indicates a transition from smooth pancake shape to a disk surrounded with annular crown.



(a)

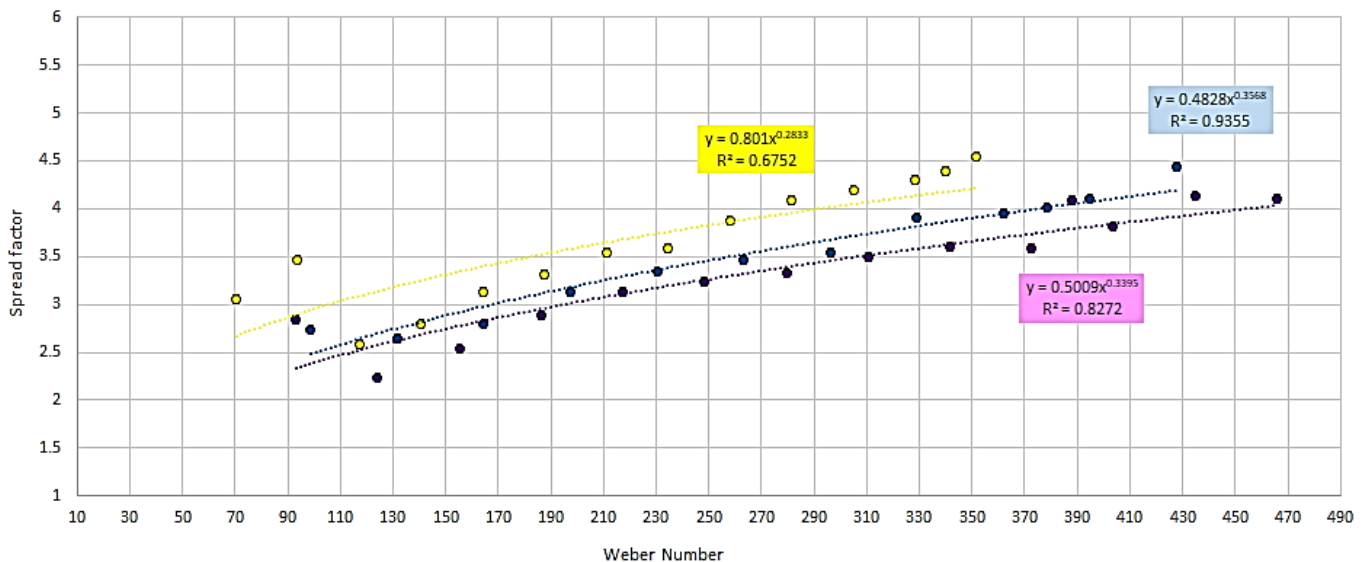


(b)

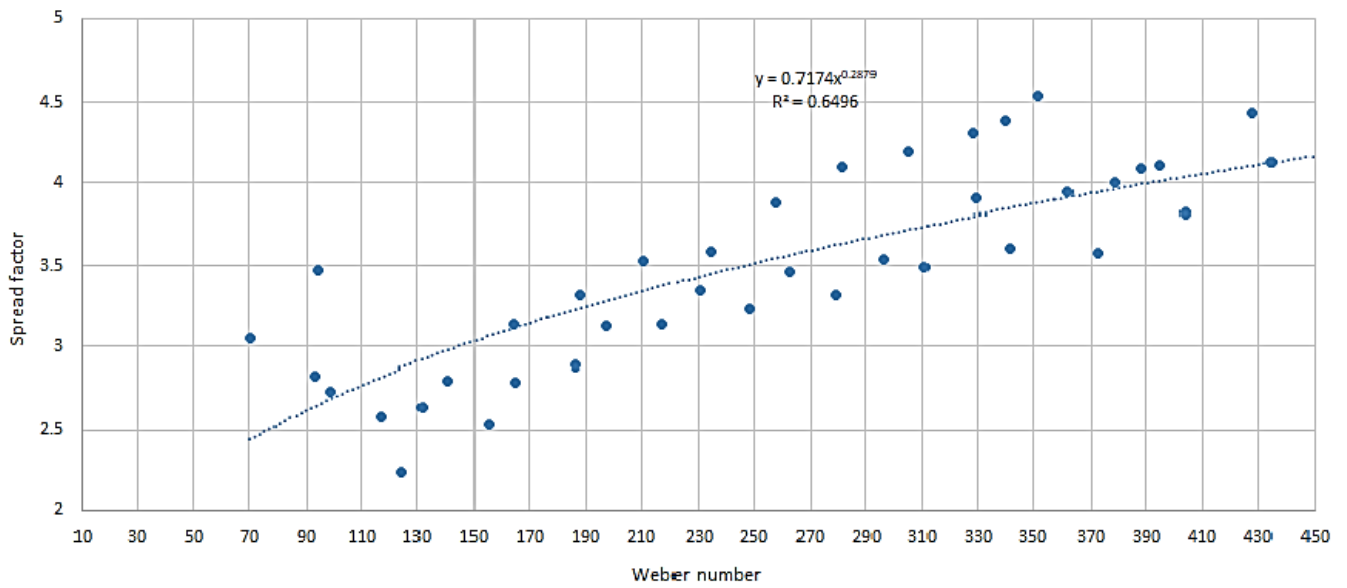
Fig. 3.2.3iii (a) Spread factor vs Weber number for all kinds of needles used for 0.1vol% nanofluid
(b) Spread factor vs Weber number for all needles combined used for 0.1vol% nanofluid

3.2.3d Spread factor vs Weber number characteristic curve for 0.5vol% nanofluid:

For dispensing the base fluid, three needles were used that had diameters of 0.714mm, 0.540mm and 0.231mm. The variation of spread factor with Weber number is shown in Fig. 3.5iv. For all the three dispensing needles, the curves are found to follow power law. The data points in the plot are aligned with the data furnished in Table 3.3d. Nanofluid droplets dispensed from the needle with minimum diameter show a non-monotonic behavior with a discontinuity around $We = 93.81$. In this case, the data points are less scattered than the previous cases and are more uniform.



(a)



(b)

Fig. 3.2.3iv (a) Spread factor vs Weber number for all kinds of needles used for 0.5vol% nanofluid
(b) Spread factor vs Weber number for all needles combined used for 0.5vol% nanofluid

Chapter-4

3. Conclusions and Future Directions:

4.1 Conclusions:

An experimental investigation has been conducted to describe the impingement dynamics of Anatase nanofluid over superhydrophobic surface. Nanofluids of three different particle volume fractions were studied, viz., $\phi=0.01$, 0.1 and 0.5%. Nanofluids were prepared by two step methods followed by sonication inside bath sonicator. Superhydrophobic aluminum surfaces were used for impinging the nanofluid droplets. Droplet impinge momentum, characterized by the Weber number, was varied by altering the droplet release height while droplet diameter was varied by using different size of dispensing needles. Salient impingement behaviors that were studied were the droplet maximum spreading diameter, its recoil, and the crowning and splashing characteristic of the post-impact droplet. It was seen that the impingement characteristic was different from that of the base fluid, and droplet impact behavior also varied with the concentration of nanoparticles in the nanofluid.

- Three sizes of needles were used for dispensing the nanofluid, viz., 0.714, 0.540 and 0.231 mm. Diameters of the dispensed droplets from these needles ranged between 0.29cm to 0.24 cm, 0.27cm to 0.22 cm and 0.19cm to 0.17 cm, respectively, depending upon the overall liquid density, surface tension and density.
- The crowning and splashing behavior were carefully observed. It was found that the Weber number for crowning and splashing increased on increasing the droplet diameter. For a low Weber number droplet dispensed from the largest diameter needle, the maximum pan-cake diameter was small and the receding was quick as compared to the high Weber number cases. For high Weber number cases, the receding of impacted droplet after the spreading phase was slow and it was accompanied by the formation of crowns and extensions at the impinged droplet perimeter.
- For the base fluid (Water), the maximum spreading diameter showed a non-monotonic trend for droplet dispensed from minimum diameter needle. A sudden transition from smooth pancake diameter to disk surrounded with annular crown may be attributed to this non-monotonicity. On the contrary, no such trend was observed for droplets dispensed from larger needles and from the same height.

- For 0.01vol% TiO_2 -CTAB nanofluid, a non-monotonic trend was observed for droplet dispensed from minimum diameter needle and also the trendline for larger needles coincided indicating common datasets.
- For 0.1vol% TiO_2 -CTAB nanofluid, the non-monotonic trend was observed for droplet dispensed from minimum diameter needle and diameter with 0.540mm.
- On using 0.5vol% TiO_2 -CTAB nanofluid, the non-monotonic behavior was observed for droplets dispensed from the minimum diameter needle. But in this case, the data points are less scattered than the previous ones.

4.2 Future Directions:

The role of nanofluid droplet impingement in industry and other applications, which includes spray cooling, ink-jet printing, etc., is unquestionably pervasive. Handling nanofluid droplets is still plagued by some practical challenges like colloidal instability, high production cost. So, choosing appropriate and right amount of surfactant is important. Droplet impingement and bouncing still remains a complex phenomenon for the researchers for comprehending and characterizing the impact, splashing and receding events. However, there are few opportunities and challenges remaining in the field.

- Behavior of nanofluid droplet impact over the heated surfaces is less studied and it can be an area of interest.
- More variation of droplet diameters with different kinds of nanoparticles with different kinds of surfactant can be studied in order to investigate the dynamic behavior of droplet impingement which can lead to the study of heat transfer mechanisms in advanced cooling system with increase in efficiency.
- With the impingement of functional nanoparticle based fluid, its surface modification can be done which has potential applications in microelectronics and sensor fabrication.
- Impingement of nanofluids over surfaces by changing the contact angle or changing the wettability of the surface can be studied, which has potential applications in areas such as inkjet printing, coating technologies (e.g., development of anti-fouling surfaces) or surface patterning.
- Impingement of nanofluids over surfaces by altering the inclination can be studied.

References:

1. Lee, S., Choi, S. U., Li, S., and Eastman, J. A. (May 1, 1999). "Measuring Thermal Conductivity of Fluids Containing Oxide Nanoparticles." ASME. J. Heat Transfer. May 1999; 121(2): 280–289. <https://doi.org/10.1115/1.2825978>
2. Zhongyi Liu, Siqi Li, Xiaolong Pan, Haisheng Fang, Mechanism study on spreading dynamics of nanofluids droplet coupled with thermal evaporation, International Journal of Heat and Mass Transfer, Volume 183, Part A, 2022, 122172, ISSN 0017-9310, <https://doi.org/10.1016/j.ijheatmasstransfer.2021.122172>
3. P. Bhattacharya, S. K. Saha, A. Yadav, P. E. Phelan, R. S. Prasher, Brownian dynamics simulation to determine the effective thermal conductivity of nanofluids, Journal of Applied Physics June 2004 95(11):6492, <https://aip.scitation.org/doi/abs/10.1063/1.1736319>
4. Yimin Xuan, Qiang Li, Heat transfer enhancement of nanofluids, International Journal of Heat and Fluid Flow, Volume 21, Issue 1, 2000, Pages 58-64, ISSN 0142-727X, [https://doi.org/10.1016/S0142-727X\(99\)00067-3](https://doi.org/10.1016/S0142-727X(99)00067-3)
5. S. U. S. Choi, Z. G. Zhang, W. Yu, F. E. Lockwood, E. A. Grulke, Anomalous thermal conductivity enhancement in nanotube suspensions, Applied Physics Letters October 2001 79(14):2252-2254, <https://doi.org/10.1063/1.1408272>
6. Wong, Kaufui V., and Omar De Leon. "Applications of nanofluids: current and future." Advances in mechanical engineering 2 (2010): 519659
7. Ines M. Hauner, Antoine Deblais, James K. Beattie, Hamid Kellay, and Daniel Bonn, The Dynamic Surface Tension of Water, The Journal of Physical Chemistry Letters 2017 8 (7), 1599-1603, <https://doi.org/10.1021/acs.jpcllett.7b00267>
8. Schmidt, F.; Steyer, H. Neue Untersuchungen über die zeitliche Änderung der Spannung reiner Wasseroberflächen. Ann. Phys. 1926, 384 (5), 442–464

9. Sibiriyakov, N, Dependence of the surfactant solutions surface tension on the concentration and on the temperature, Journal of Physics: Conference Series, 1867 012026, <https://dx.doi.org/10.1088/1742-6596/1867/1/012026>
10. The surface tension of surfactant-containing, finite volume droplets, Bzdek, Bryan R, Reid, Jonathan P, Malila, Jussi, Prisle, Nønne L, 2020/04/14, <https://doi.org/10.1073/pnas.1915660117>
11. N. L. Prisle, T. Raatikainen, A. Laaksonen, M. Bilde, Surfactants in cloud droplet activation: Mixed organic-inorganic particles. Atmos. Chem. Phys. 10, 5663–5683 (2010)
12. J. Malila, N. L. Prisle, A monolayer partitioning scheme for droplets of surfactant solutions. J. Adv. Model. Earth Syst. 10, 3233–3251 (2018)
13. Iglauer, S.; Favretto, S.; Spinosa, G.; Schena, G.; Blunt, M.J. X-ray tomography measurements of power-law cluster size distributions in sandstones. Phys. Rev. E 2010, 82, 056315
14. Fredrick, E.; Walstra, P.; Dewettinck, K. Factors governing partial coalescence in oil-in-water emulsions. Adv. Colloid Interface Sci. 2010, 153, 30–42
15. Kovalchuk, V.I.; Loglio, G.; Bykov, A.G.; Ferrari, M.; Krägel, J.; Liggieri, L.; Miller, R.; Milyaeva, O.Y.; Noskov, B.A.; Ravera, F.; Santini, E.; Schneck, E. Effect of Temperature on the Dynamic Properties of Mixed Surfactant Adsorbed Layers at the Water/Hexane Interface under Low-Gravity Conditions. *Colloids Interfaces* **2020**, *4*, 27. <https://doi.org/10.3390/colloids4030027>
16. Aveyard, R.; Binks, B.P.; Chen, J.; Esquena, J.; Fletcher, P.D.I.; Buscall, R.; Davies, S. Surface and Colloid Chemistry of Systems Containing Pure Sugar Surfactant. Langmuir 1998, 14, 4699–4709
17. Yang, J.; Pal, R. Investigation of Surfactant-Polymer Interactions Using Rheology and Surface Tension Measurements. *Polymers* **2020**, *12*, 2302. <https://doi.org/10.3390/polym12102302>

18. D. S. Zhu, S. Y. Wu, N. Wang; Surface Tension and Viscosity of Aluminum Oxide Nanofluids. *AIP Conference Proceedings* 1 March 2010; 1207 (1): 460-464. <https://doi.org/10.1063/1.3366409>
19. Xue, H. S., Fan, J. R., Hong, R. H., et al., 2007. Characteristic boiling curve of carbon nanotube nanofluid as determined by the transient calorimeter technique. *Appl. Phys. Lett.* 90, 184107
20. Kumar R, Milanova D: Effect of surface tension on nanotube nanofluids. *Appl Phys Lett* 2009, 94
21. Tanvir, S. and L. Qiao, Surface tension of Nanofluid-type fuels containing suspended nanomaterials. *Nanoscale research letters*, 2012. 7(1): p. 1-10
22. M.H.U. Bhuiyan, R. Saidur, M.A. Amalina, R.M. Mostafizur, AKMS Islam, Effect of Nanoparticles Concentration and Their Sizes on Surface Tension of Nanofluids, *Procedia Engineering*, Volume 105, 2015, Pages 431-437, ISSN 1877-7058, <https://doi.org/10.1016/j.proeng.2015.05.030>
23. Ranganathan Kumar, Denitsa Milanova; Effect of surface tension on nanotube nanofluids. *Appl. Phys. Lett.* 16 February 2009; 94 (7): 073107. <https://doi.org/10.1063/1.3085766>
24. Tanvir, S., Qiao, L. Surface tension of Nanofluid-type fuels containing suspended nanomaterials. *Nanoscale Res Lett* 7, 226 (2012). <https://doi.org/10.1186/1556-276X-7-226>
25. Murshed SMS, Milanova D, Kumar R: An experimental study of surface tension-dependent pool boiling characteristics of carbon nanotubes-nanofluids. *Book An experimental study of surface tension-dependent pool boiling characteristics of carbon nanotubes-nanofluids* 2009

26. Vafaei S, Purkayastha A, Jain A, Ramanath G, Borca-Tasciuc T: The effect of nanoparticles on the liquid-gas surface tension of Bi(2)Te(3) nanofluids. *J Colloid Interf Sci* 2009., 20
27. Chen RH, Phuoc TX, Martello D: Surface tension of evaporating nanofluid droplets. *Int J Heat Mass Tran* 2011, 54: 2459–2466. 10.1016/j.ijheatmasstransfer.2011.02.016
28. F. Ravera, E. Santini, G. Loglio, M. Ferrari, L. Liggieri, Effect of nanoparticles on the interfacial properties of liquid/liquid and liquid/air surface layers, *J. Phys. Chem. B* 110 (2006) 19543–19551
29. Pritam Kumar Das, Arnab Kumar Mallik, Ranjan Ganguly, Apurba Kumar Santra, Synthesis and characterization of TiO₂–water nanofluids with different surfactants, *International Communications in Heat and Mass Transfer*, Volume 75, 2016, Pages 341–348, ISSN 0735-1933, <https://doi.org/10.1016/j.icheatmasstransfer.2016.05.011>
30. Oliphant K, Webb B and McQuay M 1998 *Exp. Therm Fluid Sci.* 18(1) 1–10
31. Experimental Investigation of TiO₂/Water Nanofluid Droplet Impingement on Nanostructured Surfaces Mostafa Kahani, Robert Gordon Jackson, and Gary Rosengarten, *Industrial & Engineering Chemistry Research* 2016 55 (7), 2230–2241, <https://doi.org/10.1021/acs.iecr.5b04465>
32. Meibing Hu, Jiandong Zhou, Yang Li, Xin Zhuo, Dengwei Jing, Effects of the surface wettability of nanoparticles on the impact dynamics of droplets, *Chemical Engineering Science*, Volume 246, 2021, 116977, ISSN 0009-2509, <https://doi.org/10.1016/j.ces.2021.116977>
33. Semenov, S.; Trybala, A.; Rubio, R.G.; Kovalchuk, N.; Starov, V.; Velarde, M.G. Simultaneous spreading and evaporation: Recent developments. *Adv. Colloid Interface Sci.* 2014, 206, 382–398
34. Wasan, Darsh T, Nikolov, Alex D, Spreading of nanofluids on solids, *Nature* 423, 156 (2003) <https://doi.org/10.1038/nature01591>

35. Jackson, Robert Gordon, Kahani, Mostafa, Karwa, Nitin, Wu, Alex, Lamb, Robert, Taylor, Robert, Rosengarten, Gary, Effect of surface wettability on carbon nanotube water-based nanofluid droplet impingement heat transfer, Journal of Physics: Conference Series 525 (2014) 012024, <https://dx.doi.org/10.1088/1742-6596/525/1/012024>
36. Rosengarten G, Tetuko A, Li K K, Wu A and Lamb R 2011 ASME Int. Mechanical Eng. Congress, Denver
37. Bruce M. Law, Sean P. McBride, Jiang Yong Wang, Haeng Sub Wi, Govind Paneru, Santiago Betelu, Baku Ushijima, Youichi Takata, Bret Flanders, Fernando Bresme, Hiroki Matsubara, Takanori Takiue, Makoto Aratono, Line tension and its influence on droplets and particles at surfaces, Progress in Surface Science, Volume 92, Issue 1, 2017, Pages 1-39, ISSN 0079-6816, <https://doi.org/10.1016/j.progsurf.2016.12.002>
38. H.A. Barnes, J.F. Hutton, K. Walters, An Introduction to Rheology, Elsevier Science Publishers B.V., 1989
39. Shen, J.; Liburdy, J.A.; Pence, D.V.; Narayanan, V. Droplet impingement dynamics: Effect of surface temperature during boiling and non-boiling conditions. J. Phys. Condens. Matter 2009, 21, 464133
40. Joo Hyun Moon, Jae Bong Lee, Seong Hyuk Lee, Dynamic Behavior of Non-Newtonian Droplets Impinging on Solid Surfaces, MATERIALS TRANSACTIONS, 2013, Volume 54, Issue 2, Pages 260-265, Released on J-STAGE January 25, 2013, Advance online publication January 19, 2013, Online ISSN 1347-5320, Print ISSN 1345-9678, <https://doi.org/10.2320/matertrans.M2012215>
41. Meibing Hu, Yanmin Zhang, Wei Gao, Dengwei Jing, Effects of the complex interaction between nanoparticles and surfactants on the rheological properties of suspensions, Colloids and Surfaces A: Physicochemical and Engineering Aspects, Volume 588, 2020, 124377, ISSN 0927-7757, <https://doi.org/10.1016/j.colsurfa.2019.124377>

42. Wasan, D., Nikolov, A. Spreading of nanofluids on solids. *Nature* **423**, 156–159 (2003). <https://doi.org/10.1038/nature01591>
43. Jacco H. Snoeijer, Bruno Andreotti, Moving Contact Lines: Scales, Regimes, and Dynamical Transitions, Journal Article, 2013, Annual Review of Fluid Mechanics January 2013 45(1):269, 10.1146/annurev-fluid-011212-140734
44. Chun Huh, L.E Scriven, Hydrodynamic model of steady movement of a solid/liquid/fluid contact line, Journal of Colloid and Interface Science, Volume 35, Issue 1, 1971, Pages 85-101, ISSN 0021-9797, [https://doi.org/10.1016/0021-9797\(71\)90188-3](https://doi.org/10.1016/0021-9797(71)90188-3)
45. Bonn D, Eggers J, Indekeu J, Meunier J, Rolley E. 2009. Wetting and spreading. Rev. Mod. Phys. 81:739–805. <https://doi.org/10.1103/RevModPhys.81.739>
46. Blake, T. D. (1993). Dynamic contact angle and wetting kinetics. *Wettability*.
47. Hong Ren, Richard B. Fair, Michael G. Pollack, Edward J. Shaughnessy, Dynamics of electro-wetting droplet transport, Sensors and Actuators B: Chemical, Volume 87, Issue 1, 2002, Pages 201-206, ISSN 0925-4005, [https://doi.org/10.1016/S0925-4005\(02\)00223-X](https://doi.org/10.1016/S0925-4005(02)00223-X)
48. V. Bergeron, D. Bonn, J. Y. Martin and L. Vovelle, Nature, 2000, 405, 772–775
49. Hudson, N., & Jones, T. The A1 projet—an overview. *J. Non-Newtonian Fluid Mech.* **46**, 69– 88 (1993)
50. J. S. Lee, B. M. Weon, S. J. Park, J. H. Je, K. Fezzaa, and W. -K. Lee, Nature Commun. **2**, 367 (2011)
51. Kahani, M.; Jackson, R.G.; Rosengarten, G. Experimental Investigation of TiO₂/Water Nanofluid Droplet Impingement on Nanostructured Surfaces. *Ind. Eng. Chem. Res.* 2016, **55**, 2230–2241
52.] L.J. San, W. Byung Mook, J. Jung Ho, F. Kamel, How does an air film evolve into a bubble during drop impact? *Phys. Rev. Lett.* 109 (2012) 204501

53. Meibing Hu, Jiandong Zhou, Yang Li, Xin Zhuo, Dengwei Jing, Effects of the surface wettability of nanoparticles on the impact dynamics of droplets, *Chemical Engineering Science*, Volume 246, 2021, 116977, ISSN 0009-2509
54. D.C. Vadiello, A. Soucemarianadin, C. Delattre, D.C.D. Roux, Dynamic contact angle effects onto the maximum drop impact spreading on solid surfaces, *Phys. Fluids* 21 (2009) 3037
55. P.G. Pittoni, Y.C. Lin, R.J. Wang, T.S. Yu, S.Y. Lin, Bubbles entrapment for drops impinging on polymer surfaces: the roughness effect, *Exp. Thermal Fluid Sci.* 62 (2015) 183–191
56. D. Bartolo, C. Josserand, D. Bonn, Singular jets and bubbles in drop impact, *Phys. Rev. Lett.* 96 (2006) 124501
57. A.L. Yarin, Drop impact dynamics: splashing, spreading, receding, bouncing..., *Annu. Rev. Fluid Mech.* 38 (2006) 159–192
58. Li, Yang, Zhou, Jiandong, Hu, Meibing, Jing, Dengwei, Whole Contact Line Pinning for Droplets Impacting on a Hydrophobic Surface Due to Hydrophilic TiO₂ Nanoparticle Addition, *Langmuir* **2021** 37 (22), 6673-6680, <https://doi.org/10.1021/acs.langmuir.1c00523>
59. K. Sefiane, R. Bennacer, Nanofluids droplets evaporation kinetics and wetting dynamics on rough heated substrates, *Advances in Colloid and Interface Science*, Volumes 147–148, 2009, Pages 263-271, ISSN 0001-8686, <https://doi.org/10.1016/j.cis.2008.09.011>
60. Li, Y., F. Wang, H. Liu, and H. Wu, 2015, Nanoparticle-tuned spreading behavior of nanofluid droplets on the solid substrate, *Microfluid. Nanofluid.* 18, 111-120
61. D. Quéré, *Rep. Prog. Phys.* 26, 2495 (2005)
62. Shang, H. M., Wang, Y., Takahashi, K., Cao, G. Z., Li, D., & Xia, Y. N. (2005). Nanostructured superhydrophobic surfaces. *Journal of materials science*, 40(13), 3587-3591.

63. T. PHAM, J. B. JACKSON, N. J. HALAS and T. R. LEE, *Langmuir* 18 (2002) 4915
64. Maxwell, J. C. "Electricity and Magnetism Clarendon Press." (1873). 6Masuda, Hidetoshi, et al. "Alteration of thermal conductivity and viscosity of liquid by dispersing ultra-fine particles (dispersion of γ -Al₂O₃, SiO₂ and TiO₂ ultra-fine particles)." (1993)
65. Zhu, D. S., Wu, S. Y., & Wang, N. (2010, March). Surface tension and viscosity of aluminum oxide nanofluids. In *AIP Conference Proceedings* (Vol. 1207, No. 1, pp. 460-464). American Institute of Physics.
66. Radiom, M., Yang, C., & Chan, W. K. (2010, April). Characterization of surface tension and contact angle of nanofluids. In *Fourth international conference on experimental mechanics* (Vol. 7522, pp. 395-403). SPIE.
67. Han Wu, Longmin Tang, Chunze Cen, Chia-Fon Lee, Effect of droplet size on the jet breakup characteristics of n-butanol during impact on a heated surface, *Journal of Traffic and Transportation Engineering (English Edition)*, Volume 7, Issue 3, 2020, Pages 320-330, ISSN 2095-7564, <https://doi.org/10.1016/j.jtte.2020.02.001>